C. R. Mecanique 346 (2018) 57–76

Contents lists available at ScienceDirect

Comptes Rendus Mecanique

www.sciencedirect.com

A layerwise C^0-type higher order shear deformation theory for laminated composite and sandwich plates

Chien H. Thai [a,b,*], Magd Abdel Wahab [c,d,*], Hung Nguyen-Xuan [e,f]

[a] Division of Computational Mechanics, Ton Duc Thang University, Ho Chi Minh City, Vietnam
[b] Faculty of Civil Engineering, Ton Duc Thang University, Ho Chi Minh City, Vietnam
[c] Institute of Research and Development, Duy Tan University, 03 Quang Trung, Da Nang, Vietnam
[d] Soete Laboratory, Faculty of Engineering and Architecture, Ghent University, 9000, Ghent, Belgium
[e] Center for Interdisciplinary Research, Ho Chi Minh City University (Hutech), Ho Chi Minh City, Vietnam
[f] Department of Architectural Engineering, Sejong University, 209 Neungdong-ro, Gwangjin-gu, Seoul 05006, Republic of Korea

A R T I C L E   I N F O

Article history:
Received 17 July 2017
Accepted 3 November 2017
Available online 6 December 2017

Keywords:
Plate
Laminated composite
Sandwich
Layerwise C^0-type higher order shear deformation
Isogeometric analysis

A B S T R A C T

A novel layerwise C^0-type higher order shear deformation theory (layerwise C^0-type HSDT) for the analysis of laminated composite and sandwich plates is proposed. A C^0-type HSDT is used in each lamina layer and the continuity of in-plane displacements and transverse shear stresses at inner-laminar layer is consolidated. The present layerwise theory retains only seven variables without increasing the number of variables when the number of lamina layers are intensified. The shear stresses through the plate thickness derived from the constitutive equation of the present theory have the same shape as those calculated from the equilibrium equation. In addition, the artificial constraints are added in the principle of virtual displacements (PVD) and are certainly fulfilled through a penalty approach. In this paper, two C^0-continuity numerical methods, such as the Finite Element Method (FEM) and Bézier isogeometric element (BIEM) are utilized to solve a discrete system of equations derived from the PVD. Several numerical examples with various geometries, aspect ratios, stiffness ratios, and boundary conditions are investigated and compared with the 3D elasticity solution, the analytical, as well as, numerical solutions based on various plate theories.

1. Introduction

Composite and sandwich plate structures have been ubiquitously applied to various engineering industries, especially aerospace, automotive, civil, and marine engineering. For the analysis and design of these structures, an accurate understanding of displacements and stresses is necessary. Herein, the transverse shear deformation is very important due to the low ratio of transverse shear modulus to axial modulus. In fact, evaluating exactly many effects of local stress fields at the interface between layers is required.

According to published research reports in the literature, various plate theories in computational mechanics for composite and sandwich structures have been developed. These theories are divided into two groups: the equivalent single layer

* Corresponding authors.
E-mail addresses: thaihoangchien@tdt.edu.vn (Chien H. Thai), magd.abdelwahab@ugent.be (M. Abdel Wahab).

https://doi.org/10.1016/j.crme.2017.11.001
1631-0721/

approach (ESL) and the layerwise approach (LW). On the one hand, ESL assumes that the number of unknowns is independent of the number of layers. Three kinds of ESL consisting of the classical laminated plate theory (CLPT), the first-order shear deformation theory (FSDT) [1,2] and the higher-order shear deformation theory (HSDT) are usually used [3–10]. The first one remains inaccurate for laminated composite plates because it does not take into account the effects of transverse shear strains. The second one needs a shear correction factor due to a constant of transverse shear stresses through the plate thickness. It is very difficult to determine an optimized value for shear correction factors that depend on the material properties, geometries, and boundary conditions of the problems [11]. For the third type, third-order shear deformation theory (TSDT) [12], fifth-order shear deformation theory (FiSDT) [13], seventh-order shear deformation theory [14], trigonometric shear deformation theory [15–18], exponential shear deformation theory (ESDT) [19,20], and so on, provide more accurate results, yet transverse shear stress continuity conditions at the interfaces between layers are infringed. To overcome this limitation of the ESL, the LW theory has been proposed. In the LW, the number of variables or degrees of freedom (DOFs) depends on the number of layers. Therefore, the computational cost is very significant when the number of layers are increased. Some contributions of LWs have been published [21–23]. The LW proposed by Reddy [23] is widely used for laminated and sandwich structure analysis. For more detail of various shear deformation theories using the ELS and LW, some literature reviews [24–29] have been clearly presented.

In order to improve the accuracy of ESL approach and to avoid the additional computational cost of LW approach, an alternative approach, namely the refined model, has been developed. Based on the physical properties and on some mathematical transformations, the number of unknowns in the refined model becomes independent of the number of layers. Ambartsumyan [30] proposed a quadratic variation of the transverse stresses in each layer for symmetric laminated composites with arbitrary angle-ply laminate. This work was later extended by Whitney [31]. Moreover, a family of refined models denoted zigzag models were derived by Lee et al. [32], Sciuva and Icardi [33] and Kapuria et al. [34]. A good document of multilayered structures based on refined models is given by Carrera [35,36]. In addition, the refined models using the Sinus model were developed by Vidal and Polit [37–40]. A different layerwise theory that assumes the FSDT in each layer and the imposition of displacement continuity at the layers interfaces, was given by Ferreira [41]. It was latterly also developed for the laminated composite plates [42,43]. In addition, another layerwise theory was presented by Arya [44] for laminated composite beams. After that, it was extended to the analysis of laminated composite plates [45,46]. It was observed that almost all of these layerwise theories requested the C^1-continuity of the transverse displacement field. This leads to difficulties for the standard finite element method.

In this paper, we promote a layerwise theory that only requires the C^0-continuity. The method is general and is well suited to any numerical methods. The efficiency of the one presented in this paper is enhanced by using a Bézier isogeometric finite element (BIEM) for analysis. The proposed theory uses a fixed number of seven variables per node and does not increase unknowns when increasing the number of lamina layers. As a result, the present method achieves more benefits than other layerwise theories. The obtained results are evaluated by comparisons with the exact 3D theory, classical layerwise theories, and other shear deformation theories.

The paper is outlined as follows. The next section presents a layerwise C^0-type HSDT for laminated composite plates. An approximation formula based on FEM and BIEM is described in section 3. Section 4 shows numerical results and discussions. Finally, section 5 summarizes the paper with some concluding remarks.

2. On a generalized layerwise C^0-type higher-order shear deformation theory

2.1. Displacements, strains, and stresses in the plates

A layerwise higher-order shear deformation theory with any distributed functions through plate thickness was proposed by Thai et al. [46]. The displacement field at any point of the kth layer can be defined as:

$$\bar{\mathbf{u}}^k(x, y, z) = \mathbf{u}_0(x, y) + z\mathbf{u}_1(x, y) + f(z)\mathbf{u}_2(x, y) \tag{1}$$

where

$$\bar{\mathbf{u}}^k = \begin{Bmatrix} u^k \\ v^k \\ w \end{Bmatrix}; \quad \mathbf{u}_0 = \begin{Bmatrix} u_0 + A^k\phi_x \\ v_0 + C^k\phi_y \\ w_0 \end{Bmatrix}; \quad \mathbf{u}_1 = \begin{Bmatrix} -\frac{\partial w_0}{\partial x} + B^k\phi_x \\ -\frac{\partial w_0}{\partial y} + D^k\phi_y \\ 0 \end{Bmatrix}; \quad \mathbf{u}_2 = \begin{Bmatrix} \phi_x \\ \phi_y \\ 0 \end{Bmatrix} \tag{2}$$

in which u^k and v^k are the in-plane displacements at any point (x^k, y^k, z) of the layer k, and u_0, v_0, w_0, ϕ_x, and ϕ_y are the displacement components at the mid-plane of the plate in the x, y, z directions and the rotations in the y- and the x-axes, as shown in Fig. 1, respectively.

The displacement fields in Eq. (2) require the C^1-continuity of the transverse displacement. The C^1 continuity requirement can be relaxed up to C^0 by introducing two extra variables β_x and β_y with enforcements of $\frac{\partial w_0}{\partial x}$ and $\frac{\partial w_0}{\partial y}$ in Eq. (2), i.e.:

$$\frac{\partial w_0}{\partial x} = \beta_x \quad \text{and} \quad \frac{\partial w_0}{\partial y} = \beta_y \tag{3}$$

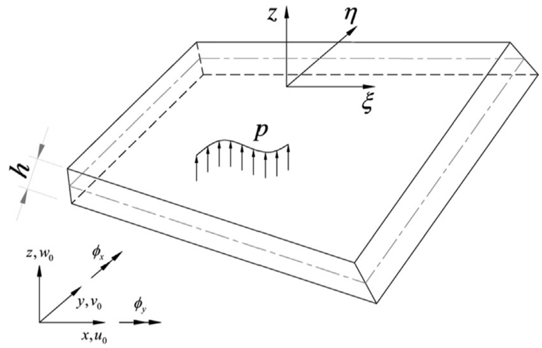

Fig. 1. Geometry of a typical plate.

In order to ensure the C^0-continuous requirement, the artificial constraints ($\frac{\partial w_0}{\partial x} - \beta_x = 0$ and $\frac{\partial w_0}{\partial y} - \beta_y = 0$) due to two additional variables are then given in the weak-form differential equations through a penalty approach.

Substituting Eq. (3) into Eq. (2), the displacement field based on a layerwise C^0-type higher order shear deformation theory is described as:

$$\mathbf{u}_0 = \begin{Bmatrix} u_0 + A^k\phi_x \\ v_0 + C^k\phi_y \\ w_0 \end{Bmatrix}; \qquad \mathbf{u}_1 = \begin{Bmatrix} -\beta_x + B^k\phi_x \\ -\beta_y + D^k\phi_y \\ 0 \end{Bmatrix}; \qquad \mathbf{u}_2 = \begin{Bmatrix} \phi_x \\ \phi_y \\ 0 \end{Bmatrix} \tag{4}$$

Imposing the continuous condition of the in-plane displacements at each layer interface as:

$$\begin{aligned} u^{k-1}(x,y,z) &= u^k(x,y,z) \\ v^{k-1}(x,y,z) &= v^k(x,y,z) \end{aligned} \tag{5}$$

From Eqs. (5) and (1), two parameters A^k and C^k can be determined as:

$$\begin{cases} A^k = A^{k-1} + z\left(B^{k-1} - B^k\right) \\ C^k = C^{k-1} + z\left(D^{k-1} - D^k\right) \end{cases} \tag{6}$$

in which the two parameters B^k and D^k will be defined later.

The relations of displacements and bending strain of the kth lamina are described as:

$$\boldsymbol{\varepsilon} = \left\{ \varepsilon_{xx} \quad \varepsilon_{yy} \quad \gamma_{xy} \right\}^{\mathrm{T}} = \boldsymbol{\varepsilon}_0 + z\boldsymbol{\varepsilon}_1 + f(z)\boldsymbol{\varepsilon}_2 \tag{7}$$

where

$$\begin{aligned} &\boldsymbol{\varepsilon}_0 = \boldsymbol{\varepsilon}_0^1 + A^k\boldsymbol{\varepsilon}_0^2 + C^k\boldsymbol{\varepsilon}_0^3; \qquad \boldsymbol{\varepsilon}_1 = \boldsymbol{\varepsilon}_1^1 + B^k\boldsymbol{\varepsilon}_1^2 + D^k\boldsymbol{\varepsilon}_1^3 \\ &\boldsymbol{\varepsilon}_0^1 = \begin{Bmatrix} u_{0,x} \\ v_{0,y} \\ u_{0,y} + v_{0,x} \end{Bmatrix}; \quad \boldsymbol{\varepsilon}_0^2 = \begin{Bmatrix} \phi_{x,x} \\ 0 \\ \phi_{x,y} \end{Bmatrix}; \quad \boldsymbol{\varepsilon}_0^3 = \begin{Bmatrix} 0 \\ \phi_{y,y} \\ \phi_{y,x} \end{Bmatrix} \\ &\boldsymbol{\varepsilon}_1^1 = -\begin{Bmatrix} \beta_{x,x} \\ \beta_{y,y} \\ \beta_{x,y} + \beta_{y,x} \end{Bmatrix}; \quad \boldsymbol{\varepsilon}_1^2 = \begin{Bmatrix} \phi_{x,x} \\ 0 \\ \phi_{x,y} \end{Bmatrix}; \quad \boldsymbol{\varepsilon}_1^3 = \begin{Bmatrix} 0 \\ \phi_{y,y} \\ \phi_{y,x} \end{Bmatrix} \quad \text{and} \quad \boldsymbol{\varepsilon}_2 = \begin{Bmatrix} \phi_{x,x} \\ \phi_{y,y} \\ \phi_{x,y} + \phi_{y,x} \end{Bmatrix} \end{aligned} \tag{8}$$

The relations of displacements and shear strain of the kth lamina are also given as follows:

$$\boldsymbol{\gamma} = \left\{ \gamma_{xz} \quad \gamma_{yz} \right\}^{\mathrm{T}} = \boldsymbol{\varepsilon}_0^s + \boldsymbol{\varepsilon}_1^s + f'(z)\boldsymbol{\varepsilon}_2^s \tag{9}$$

$$\boldsymbol{\varepsilon}_0^s = \begin{Bmatrix} w_{0,x} - \beta_x \\ w_{0,y} - \beta_y \end{Bmatrix}; \quad \boldsymbol{\varepsilon}_1^s = B^k\boldsymbol{\varepsilon}_{11}^s + D^k\boldsymbol{\varepsilon}_{12}^s; \quad \boldsymbol{\varepsilon}_{11}^s = \begin{Bmatrix} \phi_x \\ 0 \end{Bmatrix}; \quad \boldsymbol{\varepsilon}_{12}^s = \begin{Bmatrix} 0 \\ \phi_y \end{Bmatrix}; \quad \boldsymbol{\varepsilon}_2^s = \begin{Bmatrix} \phi_x \\ \phi_y \end{Bmatrix} \tag{10}$$

in which the function $f'(z)$ is the derivative of the function $f(z)$. The shape function $f(z)$ is chosen so that the shear stresses on the top and bottom surfaces of the plate are equal to zero. Without loss of generality, the third-order function proposed by Reddy [12] can be chosen as:

$$f(z) = z - \frac{4z^3}{3h^2} \quad \text{and} \quad f'(z) = 1 - \frac{4z^2}{h^2} \tag{11}$$

In this paper, the transverse normal stress is assumed to be equal to zero ($\sigma_z = 0$) due to the transverse displacement in the mid-plane surface. Applying Hooke's law to the local coordinate system, the constitutive equation of an orthotropic layer is presented by:

$$\begin{Bmatrix} \sigma_1^{(k)} \\ \sigma_2^{(k)} \\ \tau_{12}^{(k)} \\ \tau_{13}^{(k)} \\ \tau_{23}^{(k)} \end{Bmatrix} = \begin{bmatrix} Q_{11}^{(k)} & Q_{12}^{(k)} & 0 & 0 & 0 \\ Q_{21}^{(k)} & Q_{22}^{(k)} & 0 & 0 & 0 \\ 0 & 0 & Q_{66}^{(k)} & 0 & 0 \\ 0 & 0 & 0 & Q_{55}^{(k)} & 0 \\ 0 & 0 & 0 & 0 & Q_{44}^{(k)} \end{bmatrix} \begin{Bmatrix} \varepsilon_1^{(k)} \\ \varepsilon_2^{(k)} \\ \gamma_{12}^{(k)} \\ \gamma_{13}^{(k)} \\ \gamma_{23}^{(k)} \end{Bmatrix} \tag{12}$$

where subscripts 1 and 2 are the directions of the fiber and in-plane normal to fiber, respectively while subscript 3 indicates the direction normal to the plate, in which $Q_{ij}^{(k)}$ is defined as:

$$\begin{aligned} &Q_{11}^{(k)} = \frac{E_1^{(k)}}{1-\nu_{12}^{(k)}\nu_{21}^{(k)}}, \qquad Q_{12}^{(k)} = \frac{\nu_{12}^{(k)}E_2^{(k)}}{1-\nu_{12}^{(k)}\nu_{21}^{(k)}}, \qquad Q_{22}^{(k)} = \frac{E_2^{(k)}}{1-\nu_{12}^{(k)}\nu_{21}^{(k)}} \\ &Q_{66}^{(k)} = G_{12}^{(k)}, \qquad Q_{55}^{(k)} = G_{13}^{(k)}, \qquad Q_{44}^{(k)} = G_{23}^{(k)} \end{aligned} \tag{13}$$

where $E_1^{(k)}$, $E_2^{(k)}$ are the Young modulus in the 1 and 2 directions, respectively, and $G_{12}^{(k)}$, $G_{23}^{(k)}$, $G_{13}^{(k)}$ are the shear modulus in the 1–2, 2–3 and 1–3 planes, respectively, and $\nu_{12}^{(k)}$ and $\nu_{21}^{(k)}$ are Poisson's ratios.

The transverse shear stresses of every lamina layer in Eq. (12) can be rewritten as:

$$\begin{cases} \tau_{13}^k = Q_{55}^k\gamma_{13}^k = Q_{55}^k\left(w_{0,x} - \beta_x + B^k\phi_x + f'(z)\phi_x\right) \\ \tau_{23}^k = Q_{44}^k\gamma_{23}^k = Q_{44}^k\left(w_{0,y} - \beta_y + D^k\phi_y + f'(z)\phi_y\right) \end{cases} \tag{14}$$

At each layer interface, we impose the continuous condition of transverse shear stresses using:

$$\begin{cases} \tau_{13}^{k-1} = \tau_{13}^k \\ \tau_{23}^{k-1} = \tau_{23}^k \end{cases} \Rightarrow \begin{cases} Q_{55}^{k-1}\left(w_{0,x} - \beta_x + B^{k-1}\phi_x + f'(z)\phi_x\right) = Q_{55}^k\left(w_{0,x} - \beta_x + B^k\phi_x + f'(z)\phi_x\right) \\ Q_{44}^{k-1}\left(w_{0,y} - \beta_y + D^{k-1}\phi_y + f'(z)\phi_y\right) = Q_{44}^k\left(w_{0,y} - \beta_y + D^k\phi_y + f'(z)\phi_y\right) \end{cases} \tag{15}$$

Substituting Eq. (3) into Eq. (15), this equation can be written under a compact form as:

$$\Rightarrow \begin{cases} B^k = \dfrac{Q_{55}^{k-1}}{Q_{55}^k}B^{k-1} + f'(z)\left(\dfrac{Q_{55}^{k-1}}{Q_{55}^k} - 1\right) \\ D^k = \dfrac{Q_{44}^{k-1}}{Q_{44}^k}D^{k-1} + f'(z)\left(\dfrac{Q_{44}^{k-1}}{Q_{44}^k} - 1\right) \end{cases} \tag{16}$$

Thus, the four parameters A^k, B^k, C^k, and D^k in Eq. (2) that are defined (see Eq. (6) and Eq. (16)) can be rewritten as follows:

$$\begin{aligned} &B^k = \frac{Q_{55}^{k-1}}{Q_{55}^k}B^{k-1} + f'(z)\left(\frac{Q_{55}^{k-1}}{Q_{55}^k} - 1\right), \qquad A^k = A^{k-1} + z^k\left(B^{k-1} - B^k\right), \\ &D^k = \frac{Q_{44}^{k-1}}{Q_{44}^k}D^{k-1} + f'(z)\left(\frac{Q_{44}^{k-1}}{Q_{44}^k} - 1\right) \quad \text{and} \quad C^k = C^{k-1} + z^k\left(D^{k-1} - D^k\right) \end{aligned} \tag{17}$$

According to Roque et al. [45], four parameters of the first layer of symmetric laminates are obtained as:

$$B^1 = 0, \qquad A^1 = -\sum_{i=2}^{k_{\text{midplane}}} z(i)\left(B^{i-1} - B^i\right), \qquad D^1 = 0 \quad \text{and} \quad C^1 = -\sum_{i=2}^{k_{\text{midplane}}} z(i)\left(D^{i-1} - D^i\right) \tag{18}$$

Practically, the laminate is usually fabricated by several orthotropic layers and each layer must be transformed into the global coordinate system (x, y, z). A relationship of stress and strain is given by:

$$\begin{Bmatrix} \sigma_{xx}^{(k)} \\ \sigma_{yy}^{(k)} \\ \tau_{xy}^{(k)} \\ \tau_{xz}^{(k)} \\ \tau_{yz}^{(k)} \end{Bmatrix} = \begin{bmatrix} \bar{Q}_{11}^{(k)} & \bar{Q}_{12}^{(k)} & \bar{Q}_{16}^{(k)} & 0 & 0 \\ \bar{Q}_{21}^{(k)} & \bar{Q}_{22}^{(k)} & \bar{Q}_{26}^{(k)} & 0 & 0 \\ \bar{Q}_{61}^{(k)} & \bar{Q}_{62}^{(k)} & \bar{Q}_{66}^{(k)} & 0 & 0 \\ 0 & 0 & 0 & \bar{Q}_{55}^{(k)} & \bar{Q}_{54}^{(k)} \\ 0 & 0 & 0 & \bar{Q}_{45}^{(k)} & \bar{Q}_{44}^{(k)} \end{bmatrix} \begin{Bmatrix} \varepsilon_{xx}^{(k)} \\ \varepsilon_{yy}^{(k)} \\ \gamma_{xy}^{(k)} \\ \gamma_{xz}^{(k)} \\ \gamma_{yz}^{(k)} \end{Bmatrix} \tag{19}$$

where $\bar{Q}_{ij}^{(k)}$ is transformed material constant. A detailed presentation is introduced in [47].

2.2. Weak form

The strain energy associated with the artificial constraints can be added to the weak form by the Lagrange multiplier method, the penalty function method. In this paper, the penalty function method through the penalty parameter λ (e.g., Eq. (20)) is used to impose the artificial constraints so that the displacement fields ensure the C^0-continuity requirement and no additional variables are introduced. This penalty parameter is determined using the engineer's numerical experience.

For static bending problems, a weak form of the plate under transverse loading q_0 based on the present theory combined with the penalty function method can be given by:

$$\int_\Omega \delta \begin{Bmatrix} \boldsymbol{\varepsilon}_0 \\ \boldsymbol{\varepsilon}_1 \\ \boldsymbol{\varepsilon}_2 \end{Bmatrix}^{\mathrm{T}} \begin{bmatrix} \mathbf{A} & \mathbf{B} & \mathbf{E} \\ \mathbf{B} & \mathbf{D} & \mathbf{F1} \\ \mathbf{E} & \mathbf{F1} & \mathbf{H} \end{bmatrix}^{(k)} \begin{Bmatrix} \boldsymbol{\varepsilon}_0 \\ \boldsymbol{\varepsilon}_1 \\ \boldsymbol{\varepsilon}_2 \end{Bmatrix} \mathrm{d}\Omega + \int_\Omega \delta \begin{Bmatrix} \boldsymbol{\varepsilon}_0^{\mathrm{s}} \\ \boldsymbol{\varepsilon}_1^{\mathrm{s}} \end{Bmatrix}^{\mathrm{T}} \begin{bmatrix} \mathbf{A}^{\mathrm{s}} & \mathbf{B}^{\mathrm{s}} \\ \mathbf{B}^{\mathrm{s}} & \mathbf{D}^{\mathrm{s}} \end{bmatrix}^{(k)} \begin{Bmatrix} \boldsymbol{\varepsilon}_0^{\mathrm{s}} \\ \boldsymbol{\varepsilon}_1^{\mathrm{s}} \end{Bmatrix} \mathrm{d}\Omega + \lambda \int_\Omega \delta \mathbf{u}_{\mathrm{p}}^{\mathrm{T}} \mathbf{u}_{\mathrm{p}} \, \mathrm{d}\Omega$$
$$= \int_\Omega \delta w_0 q_0 \, \mathrm{d}\Omega \tag{20}$$

where

$$\mathbf{u}_{\mathrm{p}} = \left\{ \frac{\partial w_0}{\partial x} - \beta_x \quad \frac{\partial w_0}{\partial y} - \beta_y \right\}^{\mathrm{T}}$$

$$(A_{ij}, B_{ij}, D_{ij}, E_{ij}, F1_{ij}, H_{ij})^{(k)} = \int_{-h/2}^{h/2} \left(1, z, z^2, f(z), zf(z), f^2(z)\right) Q_{ij}^k \, \mathrm{d}z \quad \text{where } (i, j = 1, 2, 6) \tag{21}$$

$$\left(A_{ij}^{\mathrm{s}}, B_{ij}^{\mathrm{s}}, D_{ij}^{\mathrm{s}}\right)^{(k)} = \int_{-h/2}^{h/2} \left(1, f'(z), f'^2(z)\right) Q_{ij}^k \, \mathrm{d}z \quad \text{where } (i, j = 4, 5)$$

For free vibration problems, a weak form of the plate incorporated with the penalty function method can be described as:

$$\int_\Omega \delta \begin{Bmatrix} \boldsymbol{\varepsilon}_0 \\ \boldsymbol{\varepsilon}_1 \\ \boldsymbol{\varepsilon}_2 \end{Bmatrix}^{\mathrm{T}} \begin{bmatrix} \mathbf{A} & \mathbf{B} & \mathbf{E} \\ \mathbf{B} & \mathbf{D} & \mathbf{F1} \\ \mathbf{E} & \mathbf{F1} & \mathbf{H} \end{bmatrix}^{(k)} \begin{Bmatrix} \boldsymbol{\varepsilon}_0 \\ \boldsymbol{\varepsilon}_1 \\ \boldsymbol{\varepsilon}_2 \end{Bmatrix} \mathrm{d}\Omega + \int_\Omega \delta \begin{Bmatrix} \boldsymbol{\varepsilon}_0^{\mathrm{s}} \\ \boldsymbol{\varepsilon}_1^{\mathrm{s}} \end{Bmatrix}^{\mathrm{T}} \begin{bmatrix} \mathbf{A}^{\mathrm{s}} & \mathbf{B}^{\mathrm{s}} \\ \mathbf{B}^{\mathrm{s}} & \mathbf{D}^{\mathrm{s}} \end{bmatrix}^{(k)} \begin{Bmatrix} \boldsymbol{\varepsilon}_0^{\mathrm{s}} \\ \boldsymbol{\varepsilon}_1^{\mathrm{s}} \end{Bmatrix} \mathrm{d}\Omega + \cdots$$
$$\lambda \int_\Omega \delta \mathbf{u}_{\mathrm{p}}^{\mathrm{T}} \mathbf{u}_{\mathrm{p}} \, \mathrm{d}\Omega + \int_\Omega \delta \begin{Bmatrix} \mathbf{u}_0 \\ \mathbf{u}_1 \\ \mathbf{u}_2 \end{Bmatrix}^{\mathrm{T}} \begin{bmatrix} I_1 & I_2 & I_4 \\ I_2 & I_3 & I_5 \\ I_4 & I_5 & I_6 \end{bmatrix} \begin{Bmatrix} \ddot{\mathbf{u}}_0 \\ \ddot{\mathbf{u}}_1 \\ \ddot{\mathbf{u}}_2 \end{Bmatrix} \mathrm{d}\Omega = \mathbf{0} \tag{22}$$

where

$$(I_1, I_2, I_3, I_4, I_5, I_6)^{(k)} = \int_{-h^{(k)}/2}^{h^{(k)}/2} \rho^{(k)}(z) \left(1, z, z^2, f(z), zf(z), f^2(z)\right) \mathrm{d}z \tag{23}$$

For buckling problems under in-plane loading, a weak form of the plate combined with the penalty function method can be expressed by:

$$\int_\Omega \delta \begin{Bmatrix} \boldsymbol{\varepsilon}_0 \\ \boldsymbol{\varepsilon}_1 \\ \boldsymbol{\varepsilon}_2 \end{Bmatrix}^{\mathrm{T}} \begin{bmatrix} \mathbf{A} & \mathbf{B} & \mathbf{E} \\ \mathbf{B} & \mathbf{D} & \mathbf{F1} \\ \mathbf{E} & \mathbf{F1} & \mathbf{H} \end{bmatrix}^{(k)} \begin{Bmatrix} \boldsymbol{\varepsilon}_0 \\ \boldsymbol{\varepsilon}_1 \\ \boldsymbol{\varepsilon}_2 \end{Bmatrix} \mathrm{d}\Omega + \int_\Omega \delta \begin{Bmatrix} \boldsymbol{\varepsilon}_0^{\mathrm{s}} \\ \boldsymbol{\varepsilon}_1^{\mathrm{s}} \end{Bmatrix}^{\mathrm{T}} \begin{bmatrix} \mathbf{A}^{\mathrm{s}} & \mathbf{B}^{\mathrm{s}} \\ \mathbf{B}^{\mathrm{s}} & \mathbf{D}^{\mathrm{s}} \end{bmatrix}^{(k)} \begin{Bmatrix} \boldsymbol{\varepsilon}_0^{\mathrm{s}} \\ \boldsymbol{\varepsilon}_1^{\mathrm{s}} \end{Bmatrix} \mathrm{d}\Omega + \cdots$$
$$\lambda \int_\Omega \delta \mathbf{u}_{\mathrm{p}}^{\mathrm{T}} \mathbf{u}_{\mathrm{p}} \, \mathrm{d}\Omega + h \int_\Omega \delta \begin{Bmatrix} w_{0,x} \\ w_{0,y} \end{Bmatrix}^{\mathrm{T}} \begin{bmatrix} N_x^0 & N_{xy}^0 \\ N_{xy}^0 & N_y^0 \end{bmatrix} \begin{Bmatrix} w_{0,x} \\ w_{0,y} \end{Bmatrix} \mathrm{d}\Omega = \mathbf{0} \tag{24}$$

where N_x^0, N_y^0 and N_{xy}^0 are the pre-buckling loads in the x, y, and x–y directions, respectively.

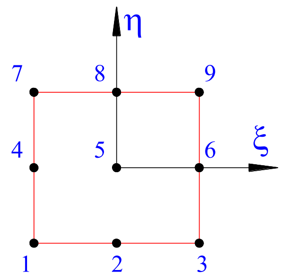

Fig. 2. A nine node isoparametric biquadratic quadrilateral element.

3. The laminated composite and sandwich plate formulation

3.1. A brief of Lagrange and Bézier extraction of NURBS functions

To investigate the proposed theory, two C^0-continuous finite and Bézier isogeometric element methods are chosen to solve discrete system equations. A brief introduction of Lagrange and Bézier extraction of NURBS functions is given in this subsection.

3.1.1. Lagrange function

Here, a nine-node isoparametric biquadratic quadrilateral is used, as shown in Fig. 2. The shape functions for a nine-node element are as follows

$$\begin{aligned}
&N_1 = \frac{1}{4}\xi\eta(\xi-1)(\eta-1); \qquad N_2 = -\frac{\eta}{2}(\eta-1)\left(\xi^2-1\right)\\
&N_3 = \frac{1}{4}\xi\eta(\xi+1)(\eta-1); \qquad N_4 = -\frac{\xi}{2}(\xi-1)\left(\eta^2-1\right)\\
&N_5 = \left(\xi^2-1\right)\left(\eta^2-1\right); \qquad N_6 = -\frac{\xi}{2}(\xi+1)\left(\eta^2-1\right)\\
&N_7 = \frac{1}{4}\xi\eta(\xi-1)(\eta+1); \qquad N_8 = -\frac{\eta}{2}\left(\xi^2-1\right)(\eta+1)\\
&N_9 = \frac{1}{4}\xi\eta(\xi+1)(\eta+1)
\end{aligned} \tag{25}$$

3.1.2. Bézier extraction of NURBS functions

In order to correspond with a nine-node finite element, the quadratic Bézier isogeometric element is used. Note that we can use other C^0-continuous Bézier isogeometric elements as described in [48].

3.2. A layerwise plate formulation based on Lagrange and Bézier extraction of NURBS basis functions

The displacement field is described by

$$\mathbf{u}^h(\xi,\eta) = \sum_{I=1}^{9} N_I(\xi,\eta)\mathbf{q}_I \tag{26}$$

where $N_I(\xi,\eta)$ is the Lagrange shape function or Bézier extraction of NURBS basis function, and $\mathbf{q}_I = \{u_{0I}\ v_{0I}\ w_{0I}\ \phi_{xI}\ \phi_{yI}\ \beta_{xI}\ \beta_{yI}\}^{\mathrm{T}}$ is the vector of nodal degrees of freedom (dofs) associated with the control point or node I.

Substituting Eq. (26) into Eq. (8), then into Eq. (7), the in-plane and shear strains can be rewritten as

$$\left\{\boldsymbol{\varepsilon}_0 \quad \boldsymbol{\varepsilon}_1 \quad \boldsymbol{\varepsilon}_2 \quad \boldsymbol{\varepsilon}_0^{\mathrm{s}} \quad \boldsymbol{\varepsilon}_1^{\mathrm{s}} \quad \boldsymbol{\varepsilon}_2^{\mathrm{s}}\right\}^{\mathrm{T}} = \sum_{I=1}^{9}\left\{\mathbf{B}_{0I} \quad \mathbf{B}_{1I} \quad \mathbf{B}_{2I} \quad \mathbf{B}_{0I}^{\mathrm{s}} \quad \mathbf{B}_{1I}^{\mathrm{s}} \quad \mathbf{B}_{2I}^{\mathrm{s}}\right\}^{\mathrm{T}}\mathbf{q}_I \tag{27}$$

in which

$$\begin{aligned}
&\mathbf{B}_{0I} = \mathbf{B}_{0I}^1 + A^k\mathbf{B}_{0I}^2 + C^k\mathbf{B}_{0I}^2; \qquad \mathbf{B}_{1I} = \mathbf{B}_{1I}^1 + B^k\mathbf{B}_{1I}^2 + D^k\mathbf{B}_{1I}^2\\
&\mathbf{B}_{0I}^1 = \begin{bmatrix} N_{I,x} & 0 & 0 & 0 & 0 & 0 & 0\\ 0 & N_{I,y} & 0 & 0 & 0 & 0 & 0\\ N_{I,y} & N_{I,x} & 0 & 0 & 0 & 0 & 0 \end{bmatrix}; \qquad \mathbf{B}_{0I}^2 = \begin{bmatrix} 0 & 0 & 0 & N_{I,x} & 0 & 0 & 0\\ 0 & 0 & 0 & 0 & 0 & 0 & 0\\ 0 & 0 & 0 & N_{I,y} & 0 & 0 & 0 \end{bmatrix}
\end{aligned} \tag{28}$$

$$\mathbf{B}_{0I}^3 = \begin{bmatrix} 0 & 0 & 0 & 0 & 0 & 0 & 0 \\ 0 & 0 & 0 & 0 & N_{I,y} & 0 & 0 \\ 0 & 0 & 0 & 0 & N_{I,x} & 0 & 0 \end{bmatrix}; \qquad \mathbf{B}_{1I}^1 = -\begin{bmatrix} 0 & 0 & 0 & 0 & 0 & N_{I,x} & 0 \\ 0 & 0 & 0 & 0 & 0 & 0 & N_{I,y} \\ 0 & 0 & 0 & 0 & 0 & N_{I,y} & N_{I,x} \end{bmatrix}$$

$$\mathbf{B}_{1I}^2 = \begin{bmatrix} 0 & 0 & 0 & 0 & N_{I,x} & 0 & 0 \\ 0 & 0 & 0 & 0 & 0 & 0 & 0 \\ 0 & 0 & 0 & 0 & N_{I,y} & 0 & 0 \end{bmatrix}; \qquad \mathbf{B}_{1I}^3 = \begin{bmatrix} 0 & 0 & 0 & 0 & 0 & 0 & 0 \\ 0 & 0 & 0 & 0 & N_{I,y} & 0 & 0 \\ 0 & 0 & 0 & 0 & N_{I,x} & 0 & 0 \end{bmatrix}$$

$$\mathbf{B}_{2I} = \begin{bmatrix} 0 & 0 & 0 & N_{I,x} & 0 & 0 & 0 \\ 0 & 0 & 0 & 0 & N_{I,y} & 0 & 0 \\ 0 & 0 & 0 & N_{I,y} & N_{I,x} & 0 & 0 \end{bmatrix}; \qquad \mathbf{B}_{1I}^{\mathrm{s}} = B^k\mathbf{B}_{11I}^{\mathrm{s}} + D^k\mathbf{B}_{12I}^{\mathrm{s}}$$

$$\mathbf{B}_{0I}^{\mathrm{s}} = \begin{bmatrix} 0 & 0 & N_{I,x} & 0 & 0 & -N_I & 0 \\ 0 & 0 & N_{I,y} & 0 & 0 & 0 & -N_I \end{bmatrix}; \qquad \mathbf{B}_{11I}^{\mathrm{s}} = \begin{bmatrix} 0 & 0 & 0 & 0 & N_I & 0 & 0 \\ 0 & 0 & 0 & 0 & 0 & 0 & 0 \end{bmatrix}$$

$$\mathbf{B}_{12I}^{\mathrm{s}} = \begin{bmatrix} 0 & 0 & 0 & 0 & 0 & 0 & 0 \\ 0 & 0 & 0 & 0 & N_I & 0 & 0 \end{bmatrix}; \qquad \mathbf{B}_{2I}^{\mathrm{s}} = \begin{bmatrix} 0 & 0 & 0 & N_I & 0 & 0 & 0 \\ 0 & 0 & 0 & 0 & N_I & 0 & 0 \end{bmatrix}$$

Substituting Eq. (26) into Eq. (4), the displacement fields $\mathbf{u}_0$, $\mathbf{u}_1$ and $\mathbf{u}_2$ can be expressed as follows:

$$\mathbf{u}_0 = \sum_{I=1}^{9}\mathbf{N}_{0I}\mathbf{q}_I; \qquad \mathbf{u}_1 = \sum_{I=1}^{9}\mathbf{N}_{1I}\mathbf{q}_I \quad \text{and} \quad \mathbf{u}_2 = \sum_{I=1}^{9}\mathbf{N}_{2I}\mathbf{q}_I \tag{29}$$

$$\mathbf{N}_{0I} = \mathbf{N}_{0I}^1 + A^k\mathbf{N}_{0I}^2 + C^k\mathbf{N}_{0I}^3; \qquad \mathbf{N}_{1I} = \mathbf{N}_{1I}^1 + B^k\mathbf{N}_{1I}^2 + D^k\mathbf{N}_{1I}^3$$

$$\mathbf{N}_{0I}^1 = \begin{bmatrix} N_I & 0 & 0 & 0 & 0 & 0 & 0 \\ 0 & N_I & 0 & 0 & 0 & 0 & 0 \\ 0 & 0 & N_I & 0 & 0 & 0 & 0 \end{bmatrix}; \qquad \mathbf{N}_{0I}^2 = \begin{bmatrix} 0 & 0 & 0 & N_I & 0 & 0 & 0 \\ 0 & 0 & 0 & 0 & 0 & 0 & 0 \\ 0 & 0 & 0 & 0 & 0 & 0 & 0 \end{bmatrix}$$

$$\mathbf{N}_{0I}^3 = \begin{bmatrix} 0 & 0 & 0 & 0 & 0 & 0 & 0 \\ 0 & 0 & 0 & 0 & N_I & 0 & 0 \\ 0 & 0 & 0 & 0 & 0 & 0 & 0 \end{bmatrix}; \qquad \mathbf{N}_{1I}^1 = -\begin{bmatrix} 0 & 0 & 0 & 0 & 0 & N_I & 0 \\ 0 & 0 & 0 & 0 & 0 & 0 & N_I \\ 0 & 0 & 0 & 0 & 0 & 0 & 0 \end{bmatrix}$$

$$\mathbf{N}_{1I}^2 = \begin{bmatrix} 0 & 0 & 0 & N_I & 0 & 0 & 0 \\ 0 & 0 & 0 & 0 & 0 & 0 & 0 \\ 0 & 0 & 0 & 0 & 0 & 0 & 0 \end{bmatrix}; \qquad \mathbf{N}_{1I}^3 = \begin{bmatrix} 0 & 0 & 0 & 0 & 0 & 0 & 0 \\ 0 & 0 & 0 & 0 & N_I & 0 & 0 \\ 0 & 0 & 0 & 0 & 0 & 0 & 0 \end{bmatrix}$$

$$\mathbf{N}_{2I} = \begin{bmatrix} 0 & 0 & 0 & N_I & 0 & 0 & 0 \\ 0 & 0 & 0 & 0 & N_I & 0 & 0 \\ 0 & 0 & 0 & 0 & 0 & 0 & 0 \end{bmatrix} \tag{30}$$

The derivations of the transverse displacements are also described by

$$\begin{Bmatrix} w_{0,x} \\ w_{0,y} \end{Bmatrix} = \sum_{I=1}^{9}\begin{bmatrix} 0 & 0 & N_{I,x} & 0 & 0 & 0 & 0 \\ 0 & 0 & N_{I,y} & 0 & 0 & 0 & 0 \end{bmatrix}\mathbf{q}_I = \sum_{I=1}^{9}\mathbf{B}_I^{\mathrm{g}}\mathbf{q}_I \tag{31}$$

The artificial constraints can be written as

$$\mathbf{u}_{\mathrm{p}} = \sum_{I=1}^{9}\mathbf{B}_{pI}\mathbf{q}_I \tag{32}$$

where

$$\mathbf{B}_{\mathrm{p}} = \begin{bmatrix} 0 & 0 & N_{I,x} & 0 & 0 & -N_I & 0 \\ 0 & 0 & N_{I,y} & 0 & 0 & 0 & -N_I \end{bmatrix} \tag{33}$$

Substituting Eqs. (27), (29), (31) and (32) into Eqs. (20), (22) and (24), respectively, the formulations of static, free vibration and buckling problems are expressed by

$$(\mathbf{K} + \lambda\mathbf{K}_{\mathrm{p}})\mathbf{q} = \mathbf{F} \tag{34}$$

$$\left(\mathbf{K} + \lambda\mathbf{K}_{\mathrm{p}} - \omega^2\mathbf{M}\right)\mathbf{q} = \mathbf{0} \tag{35}$$

$$(\mathbf{K} + \lambda\mathbf{K}_{\mathrm{p}} - \lambda_{\mathrm{cr}}\mathbf{K}_{\mathrm{g}})\mathbf{q} = \mathbf{0} \tag{36}$$

where $\mathbf{K}$, $\mathbf{K}_{\mathrm{p}}$, $\mathbf{M}$, $\mathbf{K}_{\mathrm{g}}$, $\mathbf{F}$ are the global stiffness, penalty, mass, geometric stiffness matrices, and load vector of systems, respectively, and

$$\mathbf{K}=\int_{\Omega}\left[\begin{Bmatrix}\mathbf{B}_0\\ \mathbf{B}_1\\ \mathbf{B}_2\end{Bmatrix}^{\mathrm{T}}\begin{bmatrix}\mathbf{A} & \mathbf{B} & \mathbf{E}\\ \mathbf{B} & \mathbf{D} & \mathbf{F}1\\ \mathbf{E} & \mathbf{F}1 & \mathbf{H}\end{bmatrix}\begin{Bmatrix}\mathbf{B}_0\\ \mathbf{B}_1\\ \mathbf{B}_2\end{Bmatrix}+\begin{Bmatrix}\mathbf{B}_0^{\mathrm{s}}\\ \mathbf{B}_1^{\mathrm{s}}\end{Bmatrix}^{T}\begin{bmatrix}\mathbf{A}^{\mathrm{s}} & \mathbf{B}^{\mathrm{s}}\\ \mathbf{B}^{\mathrm{s}} & \mathbf{D}^{\mathrm{s}}\end{bmatrix}\begin{Bmatrix}\mathbf{B}_0^{\mathrm{s}}\\ \mathbf{B}_1^{\mathrm{s}}\end{Bmatrix}\right]\mathrm{d}\Omega \tag{37}$$

$$\mathbf{K}_{\mathrm{p}}=\int_{\Omega}(\mathbf{B}_{\mathrm{p}})^{\mathrm{T}}\mathbf{B}_{\mathrm{p}}\,\mathrm{d}\Omega$$

$$\mathbf{F}=\int_{\Omega}q_0\left\{0\quad 0\quad N_I\quad 0\quad 0\quad 0\quad 0\right\}^{\mathrm{T}}\mathrm{d}\Omega \tag{38}$$

$$\mathbf{M}=\int_{\Omega}\begin{Bmatrix}\mathbf{N}_0\\ \mathbf{N}_1\\ \mathbf{N}_2\end{Bmatrix}^{\mathrm{T}}\begin{bmatrix}I_1 & I_2 & I_4\\ I_2 & I_3 & I_5\\ I_4 & I_5 & I_6\end{bmatrix}\begin{Bmatrix}\mathbf{N}_0\\ \mathbf{N}_1\\ \mathbf{N}_2\end{Bmatrix}\mathrm{d}\Omega \tag{39}$$

$$\mathbf{K}_{\mathrm{g}}=h\int_{\Omega}(\mathbf{B}^{\mathrm{g}})^{\mathrm{T}}\begin{bmatrix}N_x^0 & N_{xy}^0\\ N_{xy}^0 & N_y^0\end{bmatrix}\mathbf{B}^{\mathrm{g}}\,\mathrm{d}\Omega \tag{40}$$

in which ω in Eq. (35) is the natural frequency and λ_{cr} in Eq. (36) is the critical buckling value.

4. Results and discussions

In this section, some numerical results from static, buckling and vibration analyses of the laminated composite and sandwich plates are presented and discussed to show the accuracy of the present layerwise theory. The material parameters are given as follows:

- material I,

$$E_1=25E_2,\qquad G_{12}=G_{13}=0.5E_2,\qquad G_{23}=0.2E_2,\qquad \nu_{12}=0.25,\qquad \rho=1$$

- material II [49],

$$E_1=40E_2,\qquad G_{12}=G_{13}=0.6E_2,\qquad G_{23}=0.5E_2,\qquad \nu_{12}=0.25,\qquad \rho=1$$

- material III [50],

$$E_1=2.45E_2,\qquad G_{12}=G_{13}=0.48E_2,\qquad G_{23}=0.2E_2,\qquad \nu_{12}=0.23,\qquad \rho=1$$

- material IV [51],
  face layer,

$$E_1=19E_2,\qquad G_{12}=G_{13}=0.52E_2,\qquad G_{23}=0.338E_2,\qquad \nu_{12}=\nu_{13}=0.32$$

  core,

$$E_1=3.2\times10^{-5}E_2^{\mathrm{f}},\qquad E_2=32.9\times10^{-5}E_2^{\mathrm{f}},\qquad G_{12}=2.4\times10^{-3}E_2^{\mathrm{f}},\qquad G_{13}=7.9\times10^{-2}E_2^{\mathrm{f}}$$
$$G_{23}=6.6\times10^{-2}E_2^{\mathrm{f}},\qquad \nu_{12}=0.99,\qquad \nu_{13}=3.0\times10^{-5}$$

  where E_2^{f} is the Young modulus of the face layer.

4.1. Static analysis

4.1.1. Four layer [0/90/90/0] square laminated plate under sinusoidally distributed load

A cross-ply four-layer [0/90/90/0] simply supported square plate under a sinusoidally distributed load $q_0=\bar{q}_0\sin(\frac{\pi x}{a})(\frac{\pi y}{b})$ is first studied, as shown in Fig. 3a. Material I is used. The length-to-thickness ratio is taken as 4, 10, 20, and 100, respectively. The plate is modeled by 17×17 elements, as illustrated in Fig. 3b. The normalized deflection and stresses are defined by:

$$\begin{aligned}&\bar{w}=(100E_2h^3)w\left(\frac{a}{2},\frac{a}{2},0\right)/(\bar{q}_0a^4),\qquad \bar{\sigma}_x=\frac{h^2}{\bar{q}_0b^2}\sigma_x\left(\frac{a}{2},\frac{a}{2},\frac{h}{2}\right),\qquad \bar{\sigma}_y=\frac{h^2}{\bar{q}_0b^2}\sigma_y\left(\frac{a}{2},\frac{a}{2},\frac{h}{4}\right)\\ &\bar{\tau}_{xy}=\frac{h^2}{\bar{q}_0b^2}\tau_{xy}\left(0,0,\frac{h}{2}\right),\qquad \bar{\tau}_{xz}=\frac{h}{\bar{q}_0b}\tau_{xz}\left(0,\frac{a}{2},0\right),\qquad \bar{\tau}_{yz}=\frac{h}{\bar{q}_0b}\tau_{yz}\left(\frac{a}{2},0,0\right)\end{aligned} \tag{41}$$

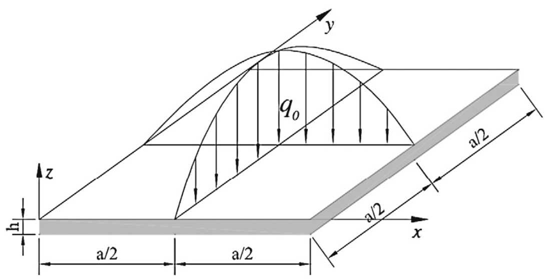

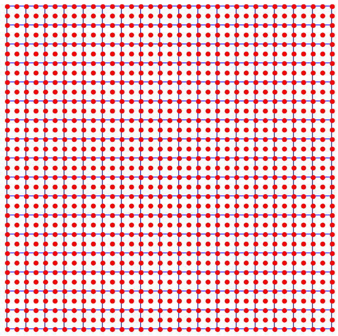

Fig. 3. A square plate: a) geometry; b) mesh element.

Table 1
The normalized displacement of the [0/90/90/0] laminated square plate ($a/h = 4$).

Method	λ					
	10^3	10^4	10^5	10^6	10^7	10^8
FEM-LW (present)	1.90566	1.90565	1.90565	1.90563	1.90566	1.90619
BIEM-LW (present)	1.90566	1.90565	1.90565	1.90565	1.90564	1.90553

Firstly, the effect of the penalty parameter (λ) through the penalty function method on the present solution is studied. The length-to-thickness ratio $a/h = 4$ is only tested, and the normalized central deflection is investigated. The penalty parameter has a value ranged between 10^3 and 10^8 (for example, $\lambda = 10^3$, 10^4, 10^5, 10^6, 10^7, 10^8). Table 1 gives the normalized central displacement of the plate corresponding with various values of penalty parameter. It can be seen that the difference for all solutions is not significant, and therefore, the penalty parameter $\lambda = 10^6$ is chosen in this study.

Next, the normalized displacement and stresses with various length-to-thickness ratios are investigated. Table 2 gives the normalized displacement and stresses of four layers simply supported square plate of the present and other solutions. The obtained results are compared with those reported by Reddy [12] based on the exact closed-form solution (CFS) and TSDT (C^1-continuity and five degrees of freedom (DOF) per node), Akhras et al. [53] based on a finite strip method (FSM) and HSDT (C^1-continuity and 5 DOFs per node), Ferreira [41] based on a meshfree method and the layerwise deformation theory (LW) with assumed FSDT for every layer (C^0-continuity and 5 DOFs per node), Roque et al. [55] based on a meshfree method and a trigonometric layerwise deformation theory (C^1-continuity and only 5 DOFs per node due to the continuity assumption of the displacement and transverse shear stresses at the layer interfaces), Wang and Shi [56] based on a closed-form solution and the third-order shear deformation theory and inter-laminar shear stress continuity (C^1-continuity and 5 DOFs per node), Thai et al. [46] based on an isogeometric analysis (IGA) and the generalized layerwise higher-order shear deformation theory (C^1-continuity and only 5 DOFs per node due to the continuity assumption of the displacement and transverse shear stresses at the layer interfaces) and Pagano [52] based on an exact 3D elasticity solution. The percentage error (%) of displacement and stresses for the case $a/h = 4$ between the exact 3D elasticity solution and other solutions are given in parenthesis. It can be seen that the percentage error from the present solution and other solutions is acceptable. The main advantage of the presented theory is the requirement of only C^0-continuity of displacement fields and the inclusion of only seven degrees of freedom for each node in the mesh without increasing the number of variables when increasing the number of lamina layers. The results obtained from Table 2 show that the present layerwise theory is more accurate when compared with the shear deformation theories, such as TSDT [12] and HSDT [53]. Similarly, it is also accurate when compared with the layerwise theory [41,55] for the thick plates ($a/h = 4$ and 10). The differences between all solutions are small for the case of thin plates. The distribution of stresses through the thickness of the plate with $a/h = 4$ and 10 based on the FEM and BIEM are plotted in Fig. 4. As it can be seen, shear stresses from the present layerwise theory are continuous at inner-laminar layers.

4.1.2. Three-layer sandwich square plate subjected to a uniform load

Let us consider a simply supported sandwich square plate subjected to a uniform transverse load q_0. The length-to-thickness ratio is taken as 10. The thickness of the core and of the two face layers are denoted by h_c and h_f, respectively and this ratio is $h_c/h_f = 8$. The material properties of the core and face layers are defined by:

Table 2
The normalized displacement and stresses of the four layer [0/90/90/0] laminated square plate under a sinusoidally distributed load.

a/h	Method	$\bar{w}$	$\bar{\sigma}_x$	$\bar{\sigma}_y$	$\bar{\sigma}_{xz}$	$\bar{\sigma}_{yz}$	$\bar{\sigma}_{xy}$
4	FEM-LW (present)	1.9056	0.7370	0.6992	0.2305	0.2298	0.0436
		(2.48%)[a]	(2.36%)	(4.98%)	(14.63%)	(21.03%)	(6.64%)
	BIEM-LW (present)	1.9056	0.7370	0.6992	0.2266	0.2259	0.0421
		(2.48%)	(2.36%)	(4.98%)	(16.07%)	(22.37%)	(9.85%)
	Elasticity [52]	1.954	0.72	0.666	0.27	0.2910	0.0467
	CFS-TSDT [12]	1.8939	0.6806	0.6463	0.2109	0.2390	0.045
		(3.08%)	(5.47%)	(2.96%)	(21.89%)	(17.87%)	(3.64%)
	FSM-HSDT [53]	1.8937	0.6651	0.6322	0.2064	–	0.044
		(3.09%)	(7.62%)	(5.08%)	(23.56%)		(5.78%)
	Meshfree-LW [41]	1.9075	0.6432	0.6228	0.2166	–	0.0441
		(2.38%)	(10.67%)	(6.49%)	(19.78%)		(5.57%)
	Meshfree-LW [55]	1.8842	0.756	0.6777	0.1885	–	0.0430
		(3.57%)	(5.00%)	(1.76%)	(30.19%)		(7.92%)
	CFS-LW [56]	1.9073	0.7361	0.6994	0.211	0.3147	0.0435
		(2.39%)	(2.24%)	(5.02%)	(21.85%)	(8.14%)	(6.85%)
	IGA-LW [46]	1.9060	0.7334	0.6984	0.2298	–	0.0434
		(2.46%)	(1.86%)	(4.86%)	(14.89%)		(7.07%)
10	FEM-LW (present)	0.7358	0.5608	0.4075	0.3156	0.1491	0.0274
	BIEM-LW (present)	0.7359	0.5608	0.4075	0.3102	0.1466	0.0265
	Elasticity [52]	0.743	0.559	0.403	0.301	0.196	0.0276
	CFS-TSDT [12]	0.7149	0.5589	0.3974	0.2697	0.153	0.0273
	FSM-HSDT [53]	0.7147	0.5456	0.3888	0.264	–	0.0268
	Meshfree-LW [41]	0.7309	0.5496	0.3956	0.2888	–	0.0273
	Meshfree-LW [55]	0.735	0.5637	0.4055	0.2908	–	0.0272
	CFS-LW [56]	0.7368	0.5609	0.4077	0.3002	0.1995	0.0274
	IGA-LW [46]	0.7359	0.5598	0.4074	0.3138	–	0.0274
20	FEM-LW (present)	0.5127	0.5429	0.3094	0.3461	0.1252	0.0231
	BIEM-LW (present)	0.5128	0.5429	0.3095	0.3402	0.1230	0.0223
	Elasticity [52]	0.517	0.543	0.309	0.328	0.156	0.023
	CFS-TSDT [12]	0.5061	0.5523	0.311	0.2883	0.123	0.0233
	FSM-HSDT [53]	0.506	0.5393	0.3043	0.2825	–	0.0228
	Meshfree-LW [41]	0.5121	0.5417	0.3056	0.3248	–	0.023
	Meshfree-LW [55]	0.5127	0.544	0.3094	0.3203	–	0.0223
	CFS-LW [56]	0.5138	0.5433	0.3098	0.3279	0.1563	0.0231
	IGA-LW [46]	0.5129	0.5425	0.3095	0.3412	–	0.023
100	FEM-LW (present)	0.4263	0.5313	0.2672	0.4448	0.1240	0.0210
	BIEM-LW (present)	0.4369	0.5429	0.2733	0.4493	0.1215	0.0208
	Elasticity [52]	0.4347	0.539	0.271	0.339	0.141	0.0214
	CFS-TSDT [12]	0.4343	0.5507	0.2769	0.2948	0.112	0.0217
	FSM-HSDT [53]	0.4343	0.5387	0.2708	0.2897	–	0.0213
	Meshfree-LW [41]	0.4374	0.542	0.2697	0.3232	–	0.0216
	Meshfree-LW [55]	0.4345	0.5388	0.271	0.3354	–	0.0213
	CFS-LW [56]	0.4355	0.5387	0.271	0.3389	0.1390	0.0214
	IGA-LW [46]	0.4346	0.5381	0.2707	0.3519	–	0.0214

[a] The percentage errors between the 3D elasticity exact solution and other solutions are given in parentheses.

$$\bar{Q}_{\text{core}} = \begin{bmatrix} 0.999781 & 0.231192 & 0 & 0 & 0 \\ 0.231192 & 0.524886 & 0 & 0 & 0 \\ 0 & 0 & 0.262931 & 0 & 0 \\ 0 & 0 & 0 & 0.266810 & 0 \\ 0 & 0 & 0 & 0 & 0.159914 \end{bmatrix} \quad \text{and} \quad \bar{Q}_{\text{face}} = R\bar{Q}_{\text{core}}$$

where R is a scale factor.

The normalized displacement and stresses of the sandwich plate are defined as follows:

$$\bar{w} = 0.999781 w\left(\frac{a}{2}, \frac{b}{2}, 0\right) \Big/ hq_0, \qquad \bar{\sigma}_x^1 = \sigma_x^1\left(\frac{a}{2}, \frac{b}{2}, \frac{h}{2}\right) \Big/ q_0, \qquad \bar{\sigma}_x^2 = \sigma_x^1\left(\frac{a}{2}, \frac{b}{2}, \frac{2h}{5}\right) \Big/ q_0$$

$$\bar{\sigma}_x^3 = \sigma_x^2\left(\frac{a}{2}, \frac{a}{2}, \frac{2h}{5}\right) \Big/ q_0, \qquad \bar{\sigma}_y^1 = \sigma_y^1\left(\frac{a}{2}, \frac{b}{2}, \frac{h}{2}\right) \Big/ q_0, \qquad \bar{\sigma}_y^2 = \sigma_y^1\left(\frac{a}{2}, \frac{b}{2}, \frac{2h}{5}\right) \Big/ q_0, \qquad \bar{\sigma}_y^3 = \sigma_y^2\left(\frac{a}{2}, \frac{b}{2}, \frac{2h}{5}\right) \Big/ q_0$$

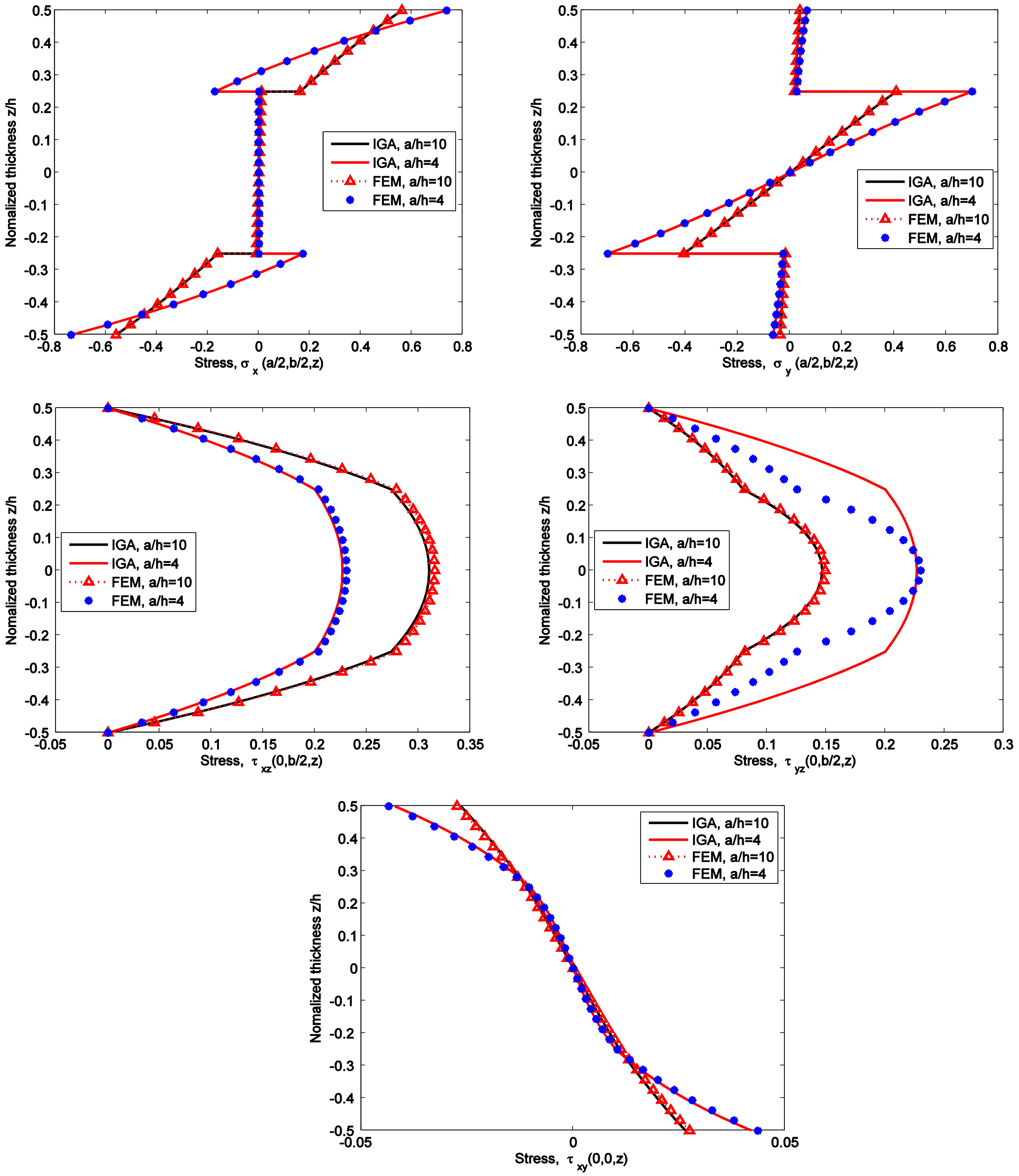

Fig. 4. The distribution of stresses through the thickness of the plate with $a/h = 4$ and 10.

In this example, three values of the scale factor, $R = 5$, 10, 15, are studied. Table 3 presents the comparison between the normalized displacement and stresses obtained by the present solution with those given by Srinivas [57] based on an analytical approach, Pandya and Kant [58] based on a finite element method (FEM) and HSDT (7 DOFs), Ferreira et al. [54] based on a meshfree method and HSDT (5 DOFs), Ferreira [41] based on a meshfree-method and LW theory (5 DOFs per node for every lamina layer), Mantari et al. [59] based on a closed form solution and trigonometric shear deformation theory (TrSDT, 5 DOFs), Grover et al. [60] based on a closed form solution and inverse hyperbolic shear deformation theory (iHSDT, 5 DOFs) and Roque et al. [55] based on a meshfree method and a trigonometric layerwise deformation theory (C^1-continuity

Table 3
The normalized displacement and stresses of the square sandwich plate under a uniform load.

R	Method	$\bar{w}$	$\bar{\sigma}_x^1$	$\bar{\sigma}_x^2$	$\bar{\sigma}_x^3$	$\bar{\sigma}_y^1$	$\bar{\sigma}_y^2$	$\bar{\sigma}_y^3$
5	FEM-LW (present)	256.6050	59.8563	46.7420	9.3484	38.2170	30.1109	6.0222
	BIEM-LW (present)	256.5896	59.8540	46.7382	9.3476	38.2160	30.1086	6.0217
	Exact [57]	258.97	60.353	46.623	9.34	38.491	30.097	6.161
	FEM-HSDT [58]	256.13	62.38	46.91	9.382	38.93	30.33	6.065
	Meshfree-HSDT [54]	257.11	60.366	47.003	9.401	38.456	30.242	6.048
	Meshfree-LW [41]	257.523	59.968	46.291	9.258	38.321	29.974	5.995
	CFS-iHSDT [60]	255.644	60.675	47.055	9.411	38.522	30.206	6.041
	CFS-TrSDT [59]	256.706	60.525	47.061	9.412	38.452	30.177	6.035
	Meshfree-LW [55]	259.12	60.338	46.57	9.314	38.547	30.148	6.0295
10	FEM-LW (present)	158.5334	64.9058	48.9612	4.8961	43.4281	33.5238	3.3524
	BIEM-LW (present)	158.5292	64.9026	48.9603	4.8960	43.4252	33.5233	3.3523
	Exact [57]	159.38	65.332	48.857	4.903	43.566	33.413	3.500
	FEM-HSDT [58]	152.33	64.65	51.31	5.131	42.83	33.97	3.397
	Meshfree-HSDT [54]	154.658	65.381	49.973	4.997	43.24	33.637	3.364
	Meshfree-LW [41]	158.38	64.846	48.443	4.844	43.39	33.306	3.924
	CFS-iHSDT [60]	154.55	65.741	49.798	4.979	43.4	33.556	3.356
	CFS-TrSDT [59]	155.498	65.542	49.708	4.971	43.385	33.591	3.359
	Meshfree-LW [55]	159.5	65.279	48.279	4.8766	43.682	33.523	3.3523
15	FEM-LW (present)	121.2461	66.3821	48.3972	3.2265	46.3437	35.1132	2.3409
	BIEM-LW (present)	121.2427	66.3808	48.3957	3.2264	46.3426	35.1122	2.3408
	Exact [57]	121.72	66.787	48.299	3.238	46.424	34.955	2.494
	FEM-HSDT [58]	110.43	66.62	51.97	3.465	44.92	35.41	2.361
	Meshfree-HSDT [54]	114.644	66.919	50.323	3.355	45.623	35.167	2.345
	Meshfree-LW [41]	120.988	66.291	47.899	3.193	46.292	34.89	2.326
	CFS-iHSDT [60]	115.82	67.272	49.813	3.321	45.967	35.088	2.339
	CFS-TrSDT [59]	115.919	67.185	49.769	3.318	45.91	35.081	2.339
	Meshfree-LW [55]	121.88	66.73	48.204	3.2136	46.586	35.109	2.3406

and only 5 DOFs per node). We showed that the obtained results are very close to those solutions for displacement as well as stresses for all values of the scale factor R. When the scale factor R increases, then the differential stiffness between the core layer and two face layers also increases and the normalized displacement decreases. For example, as $R = 15$, the present solution is better than those relying on HSDT, iHSDT and TrSDT for all displacement and in-plane stresses when compared to the exact solution.

4.2. *Buckling analysis*

In this subsection, in-plane compression uniaxial and biaxial loads are illustrated. Materials II and IV are used to compute the buckling load factor of the laminated composite and of the sandwich plates, respectively. For buckling and vibration analyses, a mesh of 11×11 elements can be used. The normalized buckling load factor is defined as:

$$\bar{\lambda} = \frac{\lambda_{\mathrm{cr}} a^2}{E_2 h^3}$$

where λ_{cr}, a, E_2, and h are the critical buckling load, the length, one of the elastic moduli of the material in the second direction, and the thickness of the plate, respectively.

4.2.1. *A laminated composite plate*

4.2.1.1. Uniaxial compression We first consider a four-layer [0/90/90/0] laminated square plate with simply supported boundary under axial compression load, as shown in Fig. 5a. Some length-to-thickness a/h and elastic modulus E_1/E_2 ratios are considered. Firstly, the length-to-thickness ratio is fixed at 10 ($a/h = 10$) and the E_1/E_2 ratio is changed. Comparisons with the 3D elasticity solution [61] and the results found in the literature as a mesh-free solution based on HSDT [62] and a FEM solution based on HSDT [63,64] are reported in Table 4. It can be noted that the obtained results show good agreement when compared to those solutions. From Table 4, a rise in the normalized critical buckling load is found when increasing the E_1/E_2 ratio. Secondly, the ratio E_1/E_2 is fixed to 40 ($E_1/E_2 = 40$), and the length-to-thickness ratio is changed. Similarly, the present results give good agreement when compared to other solution as a FEM based on FSDT [65,66] and HSDT [67], as shown in Table 5. From these two examples, it can be concluded that the obtained results of the normalized critical buckling load are very good compared to the 3D elasticity solution and to other relevant solutions.

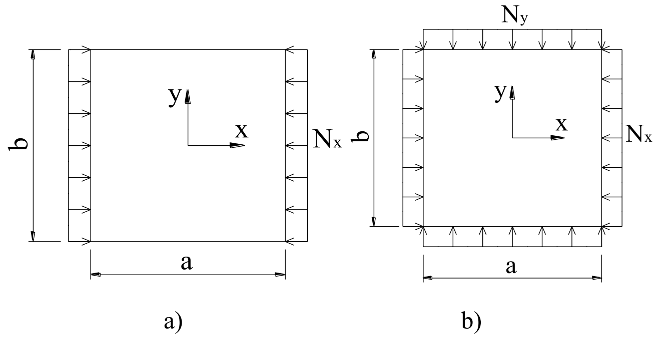

Fig. 5. Geometry of the plates under axial and biaxial compressions.

Table 4
Normalized critical buckling load of four-layer simply supported square plate with various E_1/E_2 ratios ($a/h = 10$).

Method	E_1/E_2				
	3	10	20	30	40
FEM-LW (present)	5.3947	9.9475	15.3181	19.7116	23.3981
BIEM-LW (present)	5.3940	9.9466	15.3175	19.7112	23.3976
Elasticity 3D [61]	5.294	9.762	15.019	19.304	22.881
Meshfree-HSDT [62]	5.412	10.013	15.309	19.778	23.412
FEM-HSDT [63]	5.114	9.774	15.298	19.957	23.34
FEM-HSDT [64]	5.442	10.026	15.418	19.813	23.489

Table 5
Normalized critical buckling load of four-layer simply supported square plate with various a/h ratios ($E_1/E_2 = 40$).

Method	a/h			
	10	20	50	100
FEM-LW (present)	23.3981	31.6849	35.3988	35.8723
BIEM-LW (present)	23.3976	31.6853	35.3836	35.8006
FEM-FSDT [65]	23.409	31.625	35.254	35.851
FEM-FSDT [66]	23.471	31.707	35.356	35.955
FEM-HSDT [66]	23.349	31.637	35.419	35.971

4.2.1.2. Biaxial compression Let us consider a three-layer [0/90/0] simply supported square plate subjected to the biaxial buckling load, as shown in Fig. 5b. In a fashion similar to the one described in subsection 4.2.1.1, various length-to-thickness and elastic modulus ratios are also studied to verify the normalized critical buckling load. Table 6 and Table 7 show the normalized critical buckling load under biaxial compression corresponding to fixing the value of the length-to-thickness ratio and the elastic modulus ratio, respectively. The present results are compared with the FEM based on FSDT [67] and HSDT [64] and the meshfree solution based on FSDT and HSDT [62]. The obtained results again confirmed that the present solutions including the FEM and Bézier isogeometric elements are in good agreement with other solutions for both cases.

4.2.2. The sandwich plate

The plate considered herein is an eleven-layer [0/90/0/90/0]/core/[0/90/0/90/0] sandwich square plate with simply supported boundary subjected to a uniaxial compression load. The side-to-thickness ratios are equal to 10 and 20, respectively. The ratios of the face thickness to the plate thickness are taken as $h_f/h = 0.025$, 0.05, 0.075, 0.1. The uniaxial critical buckling loads are given in Table 8. The numerical results are also compared with those reported by Noor et al. [51] based on a 3D elasticity solution, Sarah and Kant [68] based on a finite element solution using HSDT-FSDT and Cetkovic and Vuksanovic [69] based on both finite element and analytical solutions using the layerwise theory. The obtained results are in excellent agreement with those results for two kinds of plates with two side-to-thickness ratios and four values of the ratio h_f/h. Through the three examples for buckling analysis, the present theory based on the FEM and BIEM shows good agreement with all comparison results. The difference between FEM and BIEM is not significant for buckling analysis.

Table 6
Biaxial critical buckling load of three-layer [0/90/0] simply supported square plate with various modulus ratios ($a/h = 10$).

Method	E_1/E_2			
	10	20	30	40
FEM-LW (present)	4.9148	7.4428	8.8531	10.0238
BIEM-LW (present)	4.9153	7.4430	8.8532	10.0238
FEM-FSDT [67]	4.963	7.588	8.575	10.202
FEM-HSDT [64]	4.963	7.516	9.056	10.259

Table 7
Biaxial critical buckling load of three-layer [0/90/0] simply supported square plate with various ratios a/h ($E_1/E_2 = 40$).

Method	a/h				
	2	5	10	15	20
FEM-LW (present)	1.5389	5.4827	10.0238	12.0841	13.0853
BIEM-LW (present)	1.5389	5.4827	10.0238	12.0840	13.0873
Meshfree-HSDT [62]	1.457	5.519	10.251	12.239	13.164
Meshfree-FSDT [62]	1.419	5.484	10.189	12.213	13.132
FEM-HSDT [64]	1.465	5.526	10.259	12.226	13.185

Table 8
Non-dimensional critical buckling load of an eleven-layer simply supported sandwich square plate.

a/h	Method	h_f/h			
		0.025	0.05	0.075	0.1
10	FEM-LW (present)	2.2465	3.7551	4.8457	5.6956
	BIEM-LW (present)	2.2499	3.7565	4.8471	5.6953
	Elasticity [51]	2.2081	3.7385	4.8307	5.6721
	FEM-HSDT [68]	2.2122	3.7499	4.8643	5.7100
	FEM-FSDT [68]	2.2043	3.8662	5.2650	6.4930
	FEM-LW [69]	2.2592	3.7402	4.7850	5.5618
	CFS-LW [69]	2.2639	3.7649	4.8302	5.6255
20	FEM-LW (present)	2.5235	4.6557	6.3991	7.8867
	BIEM-LW (present)	2.5481	4.6539	6.4116	7.9149
	Elasticity [51]	2.5534	4.6460	6.4401	7.9352
	FEM-HSDT [68]	2.5536	4.6756	6.4528	7.9512
	FEM-FSDT [68]	2.5437	4.7128	6.6156	8.2984
	FEM-LW [69]	2.5885	4.7028	6.4604	7.9316
	CFS-LW [69]	2.5660	4.6817	6.4428	7.9184

4.3. Free vibration analysis

4.3.1. Square laminated plates

A four-layer [0/90/90/0] simply-supported square plate is first considered. In this case, the material III is used. The non-dimensional frequency is defined by $\varpi = (\omega a^2/h)(\rho/E_2)^{1/2}$, where ρ and E_2 are the mass density and the elastic modulus of the material in the second direction, respectively. The non-dimensional first frequency of a four-layer cross-ply plate with various length-to-thickness a/h and elastic modulus E_1/E_2 ratios are computed in Table 9 and Table 10, corresponding with fixed a/h and E_1/E_2 ratios, respectively. The numerical results are compared with those given by Kdheir [69] and Reddy [47] based on an analytical approach and HSDT, respectively, Liew et al. [44] based on a differential quadrature method (DQM) and FSDT, Ferreira [71,72] based on the meshfree method and FSDT, Zhen and Wanji [73] based on a triangle FEM and global–local higher order theory (GLHOT), Whu and Chen [74] based on a Fourier series expansion method (FSEM) and local higher order theory (LHOT), Matsunaga [75] based on the power series expansion and GLHOT and Cho et al. [76] based on an exact solution and layerwise theory. Good agreement is found for two cases of various length-to-thickness and elastic modulus ratios. Again, the difference between FEM and BIEM is not significant for the free vibration analysis. In the next example, the BIEM will be therefore exploited.

4.3.2. Elliptical plates

In the previous examples, we only present geometries of square plates. Several complex geometries are chosen to illustrate the effectiveness of the present solution for the free vibration analysis. In this example, let us consider a three-layer [0/90/0] laminated elliptical plate subjected to fully clamped boundary, as shown in Fig. 6a. Two radii of the elliptical plate

Table 9
A first non-dimensional frequency of four-layer simply supported square plate ($a/h = 5$).

Method-theory	E_1/E_2			
	10	20	30	40
FEM-LW (present)	8.2797	9.5461	10.3036	10.8308
BIEM-LW (present)	8.2797	9.5461	10.3036	10.8308
Meshfree-FSDT [72]	8.2526	9.4974	10.2308	10.7329
Meshfree-FSDT [71]	8.2794	9.5375	10.2889	10.8117
DQM-FSDT [49]	8.2924	9.5613	10.3200	10.8490
Exact-HSDT [70,47]	8.2982	9.5671	10.3260	10.8540

Table 10
A first non-dimensional frequency of a four-layer simply supported square plate ($E_1/E_2 = 40$).

Method-theory	a/h						
	4	5	10	20	25	50	100
FEM-LW (present)	9.3768	10.8308	15.1260	17.6535	18.0685	18.6732	19.0161
BIEM-LW (present)	9.3768	10.8308	15.1258	17.6528	18.0679	18.6826	18.8698
FEM-GLHOT [73]	9.2406	10.7294	15.1658	17.8035	18.2404	18.9022	19.1566
Fourier-LHOT [74]	9.193	10.682	15.069	17.636	18.055	18.67	18.835
FSEM-GLHOT [75]	9.1988	10.6876	15.0721	17.6369	18.0557	18.6702	18.8352
Exact-LW [76]	–	10.673	15.066	17.535	18.054	18.67	18.835

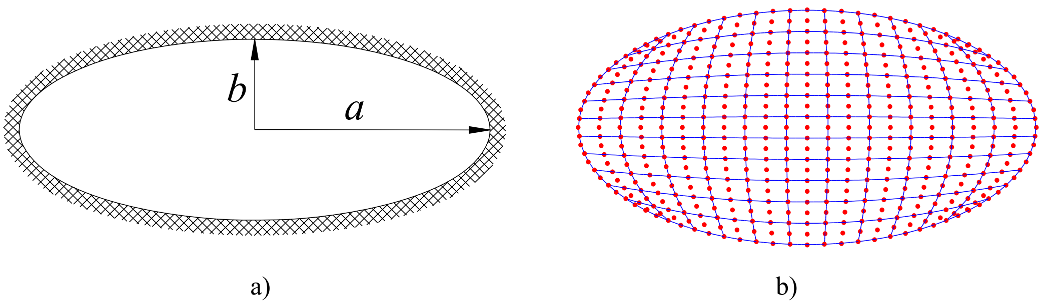

Fig. 6. Geometry and an element mesh of a clamped ellipse plate.

Table 11
First six non-dimensional frequencies of a three-layer fully clamped ellipse plate.

a/h	Method	Modes					
		1	2	3	4	5	6
5	BIEM-LW (present)	13.9384	19.6699	26.7346	28.2542	34.2643	34.6352
	IGA-LW-FSDT [43]	14.157	19.969	27.114	28.855	34.943	35.062
10	BIEM-LW (present)	17.0868	25.5616	36.8043	38.8165	48.6416	50.1563
	IGA-LW-FSDT [43]	17.184	25.714	36.982	39.196	49.148	50.259
20	BIEM-LW (present)	18.3297	28.2994	42.4716	44.3539	57.0571	60.5981
	IGA-LW-FSDT [43]	18.3290	28.28	42.255	44.321	57.09	59.827
100	BIEM-LW (present)	18.9411	29.6709	45.9757	47.6794	61.8970	68.5993
	IGA-LW-FSDT [43]	18.755	29.332	44.792	46.508	60.792	65.6230
	EFG (CLPT) [50]	18.8100	29.5800	44.9900	46.7200	61.3400	65.1400

are chosen equal to $a = 5$ and $b = 2.5$, respectively. Material III is used. The non-dimensional frequencies are given by $\varpi = (\omega a^2)(\rho h/D_0)^{1/2}$, where $D_0 = E_1 h^3/12(1 - \nu_{12}\nu_{21})$. Fig. 6b plots a mesh elliptical plate. In this example, an analytical solution is not available. Therefore, the obtained results are compared with other numerical solutions. Table 11 shows the first six non-dimensional frequencies of the elliptical plate with various radius-to-thickness ratios. The numerical results are compared with those given by Chen et al. [50] based on a meshfree method and CLPT, Thai et al. [43] based on an IGA and layerwise theory with assumed FSDT for every layer. It can be seen that a good agreement is obtained for all values of the radius-to-thickness ratio. From Table 11 it can be remarked that non-dimensional frequencies obtained from the present solution are smaller than in [43] for the thick plate (e.g., $a/h = 5$ and 10). The opposite results are obtained for

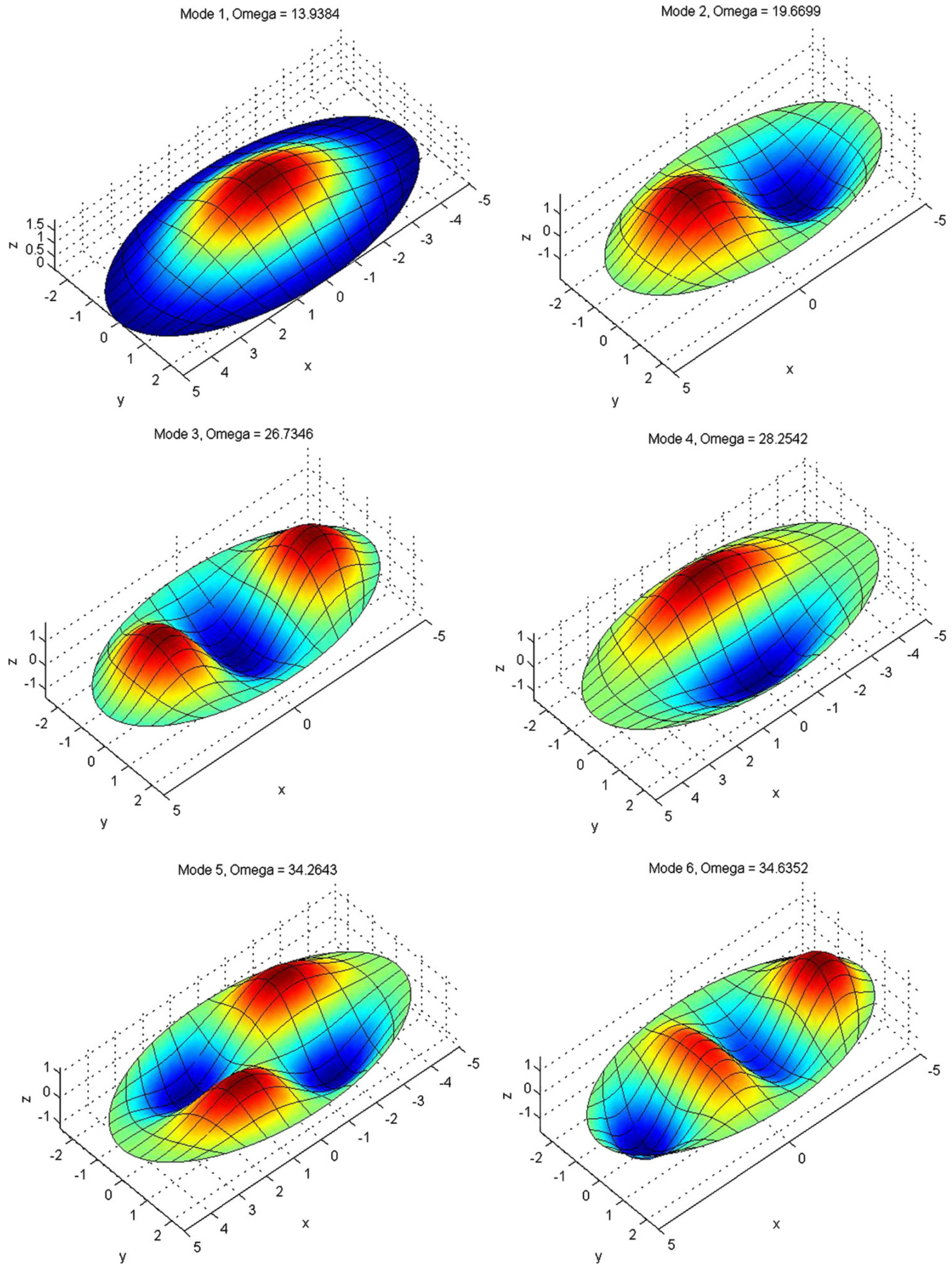

Fig. 7. The first six mode shapes of a three-layer fully clamped ellipse plate with $a/h = 5$.

the thin plate ($a/h = 100$). The first six mode shapes of a three-layer fully clamped laminated elliptical plate are plotted in Fig. 7.

4.3.3. A plate with a complicated cutout

Finally, a three-layer [0/90/0] simply supported square plate with a complicated cutout is studied, as shown in Fig. 8a. Fig. 8b plots the eight patches of the plate. The coarse mesh ($8 \times 1 \times 1$ elements) and medium mesh ($40 \times 5 \times 5$ elements) are drawn in Fig. 9. The material properties and the normalized frequencies are the same as those of example 4.3.2, where a is the length of the plate. The thickness of plate is taken as $h = 0.06$.

The first six normalized frequencies are given in Table 12. The obtained results are compared with those reported by Shojaee et al. [77] based on an IGA (quadratic and cubic elements). It is observed from Table 12 that the present solution matches well with other solutions. The first six mode shapes of the square plate with a complicated cutout are plotted in Fig. 10.

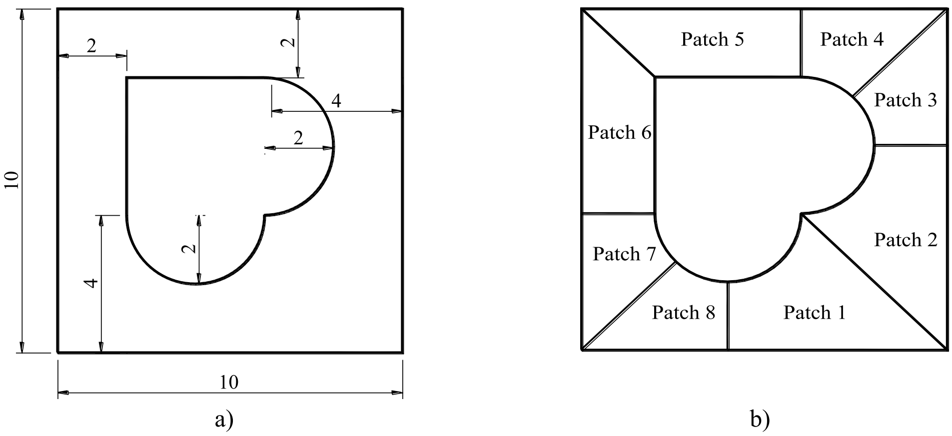

Fig. 8. The dimension of a plate and eight patches.

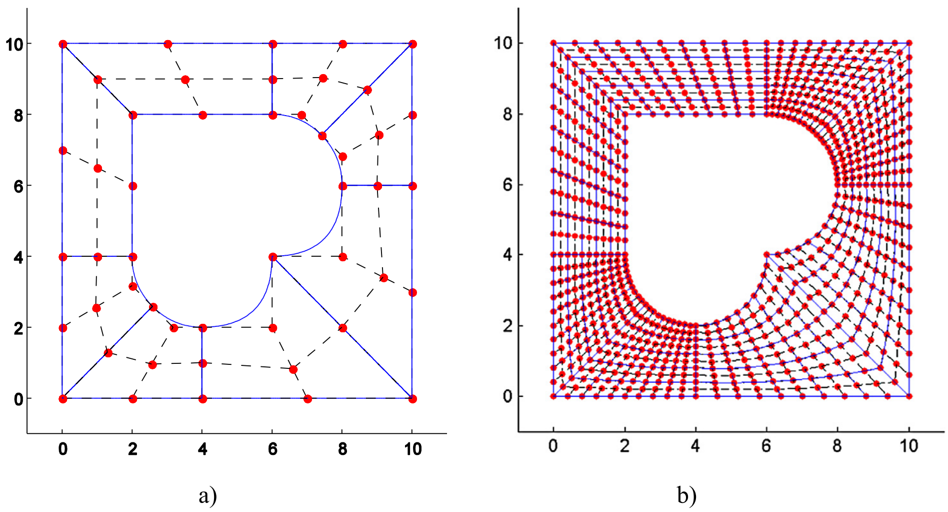

Fig. 9. a) Coarse mesh and b) medium mesh of square plate with complicated shape hole.

Table 12
Comparisons of the first six non-dimensional frequencies of a simply supported plate with cut-out complicated shape.

Method	Modes					
	1	2	3	4	5	6
BIEM-LW (present)	18.1997	31.0235	36.0375	56.6368	62.5934	84.6196
IGA-FSDT-Q [77]	18.284	31.267	35.713	55.567	62.892	82.631
IGA-FSDT-C [77]	18.190	31.087	35.655	55.452	62.582	82.383

5. Conclusions

We presented a generalized layerwise C^0-type HSDT for the analysis of laminated composite plates. The proposed layerwise theory made no changes in the number of degrees of freedom when increasing the number of lamina layers. It only required the C^0-continuity of transverse displacement field and confirmed to the traditional finite element method. The number of independent variables in the present theory is similar to that in the C^0-type HSDT, but it is capable of achieving a better accuracy of inner layer shear stresses. In addition, a penalty approach is utilized to add the artificial constraints into the PVD. Two numerical methods, i.e. the FEM and Bezier isogeometric element method, were used to investigate the present theory through numerical examples with different geometric, aspect ratios, stiffness ratios, number of layer and boundary conditions. From the obtained results, it can be concluded that the proposed theory is very suitable for static, free vibration, and buckling analyses of the laminated composite and sandwich plates. Moreover, the shear stresses through the plate thickness are equivalent to those calculated using the equilibrium equation.

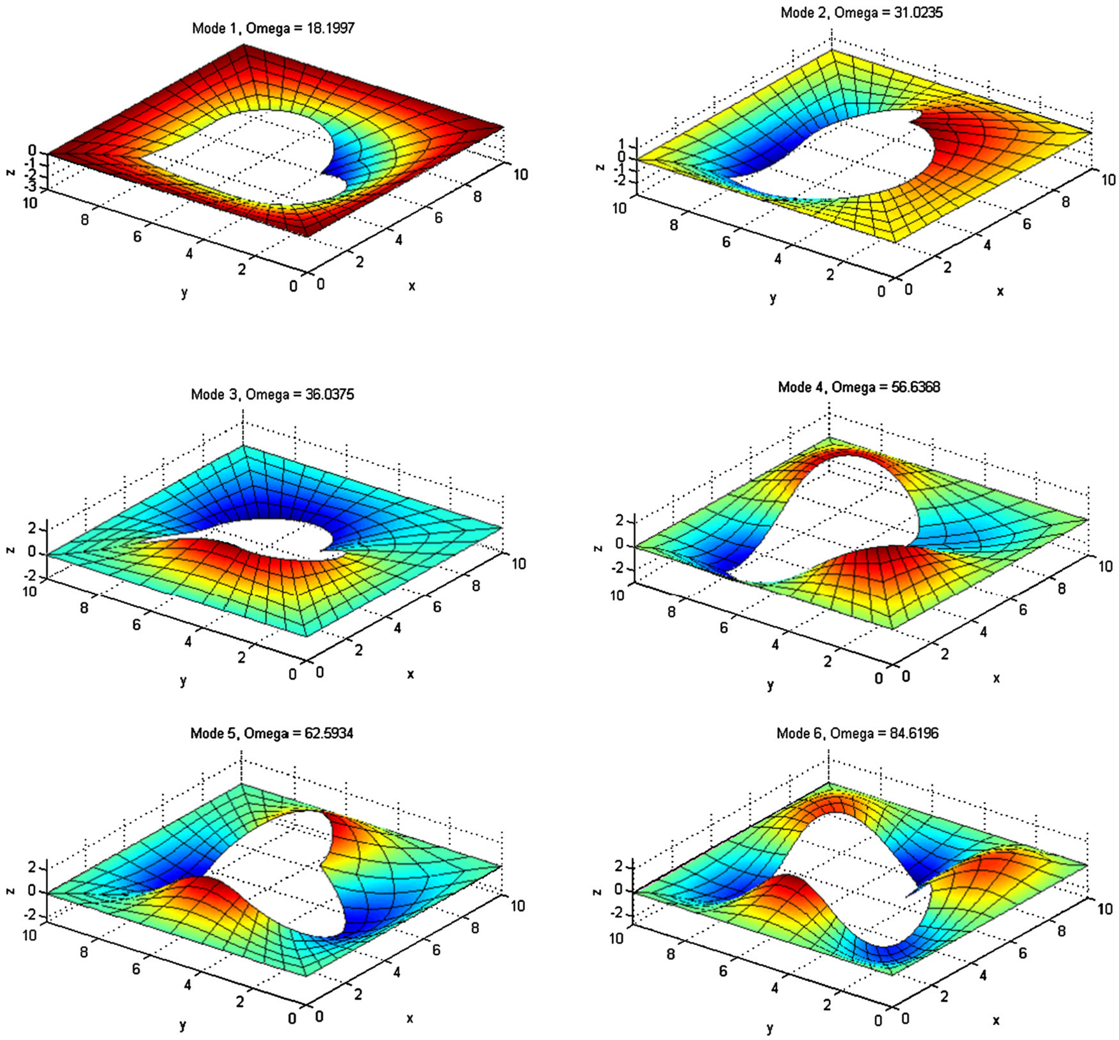

Fig. 10. The first six mode shapes of the square plate with a complicated cutout.

References

[1] E. Reissner, The effect of transverse shear deformation on the bending of elastic plates, J. Appl. Mech. 12 (1945) 69–77.

[2] R.D. Mindlin, Influence of rotary inertia and shear on flexural motions of isotropic, elastic plates, J. Appl. Mech. 18 (1951) 31–38.

[3] P. Phung-Van, L.V. Tran, A.J.M. Ferreira, H. Nguyen-Xuan, M. Abdel-Wahab, Nonlinear transient isogeometric analysis of smart piezoelectric functionally graded material plates based on generalized shear deformation theory under thermo-electro-mechanical loads, Nonlinear Dyn. 87 (2017) 879–894.

[4] L.V. Tran, P. Phung-Van, J. Lee, M.A. Wahab, H. Nguyen-Xuan, Isogeometric analysis for nonlinear thermomechanical stability of functionally graded plates, Compos. Struct. 140 (2016) 655–667.

[5] L.V. Tran, J. Lee, H.A. Ly, M.A. Wahab, H. Nguyen-Xuan, Vibration analysis of cracked FGM plates using higher-order shear deformation theory and extended isogeometric approach, Int. J. Mech. Sci. 96–97 (2015) 65–78.

[6] C.-L. Thanh, et al., Isogeometric analysis of functionally graded carbon nanotube reinforced composite nanoplates using modified couple stress theory, Compos. Struct. 184 (Supplement C) (2018) 633–649.

[7] L.V. Tran, M.A. Wahab, S.-E. Kim, An isogeometric finite element approach for thermal bending and buckling analyses of laminated composite plates, Compos. Struct. 179 (Supplement C) (2017) 35–49.

[8] P. Phung-Van, et al., An isogeometric approach for size-dependent geometrically nonlinear transient analysis of functionally graded nanoplates, Composites, Part B, Eng. 118 (2017) 125–134.

[9] P. Phung-Van, et al., Size-dependent isogeometric analysis of functionally graded carbon nanotube-reinforced composite nanoplates, Compos. Struct. 166 (2017) 120–135.

[10] X. Nguyen, et al., A refined quasi-3D isogeometric analysis for functionally graded microplates based on the modified couple stress theory, Comput. Methods Appl. Mech. Eng. 313 (2017) 904–940.

[11] A.J.M. Ferreira, L.M.S. Castro, S. Bertoluzza, A high order collocation method for the static and vibration analysis of composite plates using a first-order theory, Compos. Struct. 34 (2003) 627–636.

[12] J.N. Reddy, A simple higher-order theory for laminated composite plates, J. Appl. Mech. 51 (1984) 745–752.

[13] H. Nguyen-Xuan, C.H. Thai, T. Nguyen-Thoi, Isogeometric finite element analysis of composite sandwich plates using a higher order shear deformation theory, Composites, Part B, Eng. 55 (2013) 558–574.

[14] T.N. Nguyen, C.H. Thai, H. Nguyen-Xuan, On the general framework of high order shear deformation theories for laminated composite plate structures: a novel unified approach, Int. J. Mech. Sci. 110 (2016) 242–255.
[15] K.P. Soldatos, A transverse shear deformation theory for homogenous monoclinic plates, Acta Mech. 94 (1992) 195–220.
[16] M. Touratier, An efficient standard plate theory, Int. J. Eng. Sci. 29 (1991) 745–752.
[17] H. Arya, R.P. Shimpi, N.K. Naik, A zigzag model for laminated composite beams, Compos. Struct. 56 (2002) 21–24.
[18] Chien.H. Thai, A.J.M. Ferreira, T. Rabczuk, S.P.A. Bordas, H. Nguyen-Xuan, Isogeometric analysis of laminated composite and sandwich plates using a new inverse trigonometric shear deformation theory, Eur. J. Mech. A, Solids 43 (2014) 89–108.
[19] M. Karama, K.S. Afaq, S. Mistou, Mechanical behavior of laminated composite beam by new multi-layered laminated composite structures model with transverse shear stress continuity, Int. J. Solids Struct. 40 (2003) 1525–1546.
[20] M. Aydogdu, A new shear deformation theory for laminated composite plates, Compos. Struct. 89 (2009) 94–101.
[21] S. Srinivas, A refined analysis of composite laminates, J. Sound Vib. 30 (1973) 495–507.
[22] H. Murakami, Laminated composite plate theory with improved in-plane responses, J. Appl. Mech. 53 (1986) 661–666.
[23] J.N. Reddy, A generalization of two-dimensional theories of laminated composite plates, Commun. Appl. Numer. Methods 3 (1987) 173–180.
[24] J.N. Reddy, R.A. Arciniega, Shear deformation plate and shell theories: from Stavsky to present, Mech. Adv. Mat. Struct. 11 (2004) 535–582.
[25] J.N. Reddy, An evaluation of equivalent-single-layer and layerwise theories of composite laminates, Compos. Struct. 25 (1993) 21–35.
[26] E. Carrera, An assessment of mixed and classical theories on global and local response of multilayered orthotropic plates, Compos. Struct. 50 (2000) 183–198.
[27] E. Carrera, Theories and finite elements for multilayered, anisotropic, composite plates and shells, Arch. Comput. Methods Eng. 9 (2002) 87–140.
[28] I. Kreja, A literature review on computational models for laminated composite and sandwich panels, Centr. Eur. J. Eng. 1 (2011) 59–80.
[29] H. Altenbach, Theories for laminated and sandwich plates, Mech. Compos. Mater. 34 (1998) 243–252.
[30] S.A. Ambartsumyan, in: T. Cheron, J.E. Ashton (Eds.), Theory of Anisotropic Plates, Technomic Publishing Co, 1969, translated from Russian.
[31] J. Whitney, The effect of transverse shear deformation in the bending of laminated plates, J. Compos. Mater. 3 (1969) 534–547.
[32] C.Y. Lee, D. Liu, X. Lu, Static and vibration analysis of laminated composite beams with an interlaminar shear stress continuity theory, Int. J. Numer. Methods Eng. 33 (1992) 409–424.
[33] M.D. Sciuva, U. Icardi, Numerical assessment of the core deformability effect on the behavior of sandwich beams, Compos. Struct. 52 (2001) 41–53.
[34] S. Kapuria, P. Dumir, A. Ahmed, An efficient higher order zig-zag theory for composite and sandwich beams subjected to thermal loading, Int. J. Solids Struct. 40 (2003) 6613–6631.
[35] E. Carrera, A study of transverse normal stress effect on vibration of multilayered plates and shell, J. Sound Vib. 225 (1999) 803–829.
[36] E. Carrera, Transverse normal stress effects in multilayered plate, J. Appl. Mech. 66 (1999) 1004–1012.
[37] P. Vidal, O. Polit, A family of sinus finite elements for the analysis of rectangular laminated beams, Compos. Struct. 84 (2008) 56–72.
[38] P. Vidal, O. Polit, A refined sine-based finite element with transverse normal deformation for the analysis of laminated beams under thermomechanical loads, J. Mech. Mater. Struct. 4 (2009) 1127–1155.
[39] P. Vidal, O. Polit, A sine finite element using a zig-zag function for the analysis of laminated composite beams, Composites, Part B, Eng. 42 (2011) 1671–1682.
[40] P. Vidal, L. Gallimard, O. Polit, Proper generalized decomposition and layer-wise approach for the modeling of composite plate structures, Int. J. Solids Struct. 50 (2013) 2239–2250.
[41] A.J.M. Ferreira, Analysis of composite plates using a layerwise theory and multiquadrics discretization, Mech. Adv. Mat. Struct. 12 (2005) 99–112.
[42] A.J.M. Ferreira, G.E. Fasshauer, R.C. Batra, J.D. Rodrigues, Static deformations and vibration analysis of composite and sandwich plates using a layerwise theory and RBF-PS discretizations with optimal shape parameter, Compos. Struct. 86 (2008) 328–343.
[43] C.H. Thai, A.J.M. Ferreira, E. Carrera, H. Nguyen-Xuan, Isogeometric analysis of laminated composite and sandwich plates using a layerwise deformation theory, Compos. Struct. 104 (2013) 196–214.
[44] H. Arya, R.P. Shimpi, N.K. Naik, A zigzag model for laminated composite beams, Compos. Struct. 56 (2002) 21–24.
[45] C.M.C. Roque, A.J.M. Ferreira, R.M.N. Jorge, Modelling of composite and sandwich plates by a trigonometric layerwise deformation theory and radial basis functions, Composites, Part B, Eng. 36 (2005) 559–572.
[46] C.H. Thai, A.J.M. Ferreira, M.A. Wahab, H. Nguyen-Xuan, A generalized layerwise higher-order shear deformation theory for laminated composite and sandwich plates based on isogeometric analysis, Acta Mech. 227 (2016) 1225–1250.
[47] J.N. Reddy, Mechanics of Laminated Composite Plates, CRC Press, New York, 1997.
[48] L.B. Nguyen, C.H. Thai, H. Nguyen-Xuan, A generalized unconstrained theory and isogeometric finite element analysis based on Bézier extraction for laminated composite plates, Eng. Comput. 32 (2015) 457–475.
[49] K.M. Liew, Y.Q. Huang, J.N. Reddy, Vibration analysis of symmetrically laminated plates based on FSDT using the moving least squares differential quadrature method, Comput. Methods Appl. Mech. Eng. 192 (2003) 2203–2222.
[50] X.L. Chen, G.R. Liu, S.P. Lim, An element free Galerkin method for the free vibration analysis of composite laminates of complicated shape, Compos. Struct. 59 (2003) 279–289.
[51] A.K. Noor, J.M. Peters, W.S. Burton, Three-dimensional solutions for initially stressed structural sandwiches, J. Eng. Mech. 120 (1994) 284–303.
[52] N.J. Pagano, Exact solutions for rectangular bidirectional composites and sandwich plates, J. Compos. Mater. 4 (1970) 20–34.
[53] G. Akhras, M.S. Cheung, W. Li, Finite strip analysis for anisotropic laminated composite plates using higher-order deformation theory, Comput. Struct. 52 (1994) 471–477.
[54] A.J.M. Ferreira, C.M.C. Roque, P.A.L.S. Martins, Analysis of composite plates using higher-order shear deformation theory and a finite point formulation based on the multiquadric radial basis function method, Composites, Part B 34 (2003) 627–636.
[55] C.M.C. Roque, A.J.M. Ferreira, R.M.N. Jorge, Modelling of composite and sandwich plates by a trigonometric layerwise deformation theory and radial basis functions, Composites, Part B, Eng. 36 (2005) 559–572.
[56] X. Wang, G. Shi, A refined laminated plate theory accounting for the third-order shear deformation and interlaminar transverse stress continuity, Appl. Math. Model. 39 (2015) 5659–5680.
[57] S. Srinivas, A refined analysis of composite laminates, J. Sound Vib. 30 (1973) 495–507.
[58] B.N. Pandya, T. Kant, Higher-order shear deformable theories for flexure of sandwich plates-finite element evaluations, Int. J. Solids Struct. 24 (1988) 419–451.
[59] J.L. Mantari, A.S. Oktem, C.G. Soares, A new trigonometric shear deformation theory for isotropic, laminated composite and sandwich plates, Int. J. Solids Struct. 49 (2012).
[60] N. Grover, D.K. Maiti, B.N. Singh, A new inverse hyperbolic shear deformation theory for static and buckling analysis of laminated composite and sandwich plates, Compos. Struct. 95 (2013).
[61] A.K. Noor, Mathers, Shear-Flexible Finite Element Method of Laminated Composite Plate, Technical report, NASA, 1975.
[62] L. Liu, L.P. Chua, D.N. Ghista, Mesh-free radial basis function method for static, free vibration and buckling analysis of shear deformable composite laminates, Compos. Struct. 78 (2007) 58–69.
[63] N.D. Phan, J.N. Reddy, Analysis of laminated composite plates using a higher-order shear deformation theory, Int. J. Numer. Methods Eng. 21 (1985) 2201–2219.

[64] A.A. Khdeir, L. Librescu, Analysis of symmetric cross-ply elastic plates using a higher order theory: Part II: buckling and free vibration, Compos. Struct. 9 (1988) 259–277.
[65] A. Chakrabarti, A.H. Sheikh, Buckling of laminated composite plates by a new element based on higher order shear deformation theory, Mech. Compos. Mater. Struct. 10 (2003) 303–317.
[66] J.N. Reddy, N.D. Phan, Stability and vibration of isotropic, orthotropic and laminated plates according to a higher order shear deformation theory, J. Sound Vib. 89 (1985) 157–170.
[67] M.E. Fares, A.M. Zenkour, Buckling and free vibration of non-homogeneous composite cross-ply laminated plates with various plate theories, Compos. Struct. 44 (1999) 279–287.
[68] B. Sarah, T. Kant, Two shear deformable finite element models for buckling analysis of skew fiber-reinforced composite and sandwich panels, Compos. Struct. 46 (1999) 115–124.
[69] M. Cetkovic, D. Vuksanovic, Bending, free vibrations and buckling of laminated composite and sandwich plates using a layerwise displacement model, Compos. Struct. 88 (2009) 219–227.
[70] A. Kdheir, Analysis of symmetric cross-ply elastic plates using a higher-order theory, Part II: buckling and free vibration, Compos. Struct. 9 (1988) 259–277.
[71] A.J.M. Ferreira, L.M.S. Castro, S. Bertoluzza, A high order collocation method for the static and vibration analysis of composite plates using a first-order theory, Compos. Struct. 89 (2009) 424–432.
[72] A.J.M. Ferreira, A formulation of the multiquadric radial basis function method for the analysis of laminated composite plates, Compos. Struct. 59 (2003) 385–392.
[73] W. Zhen, C. Wanji, Free vibration of laminated composite and sandwich plates using global–local higher-order theory, J. Sound Vib. 298 (2006) 333–349.
[74] C.P. Wu, W.Y. Chen, Vibration and stability of laminated plates based on a local higher-order plate theory, J. Sound Vib. 177 (1994) 503–520.
[75] H. Matsunaga, Vibration and stability of cross-ply laminated composite plates according to a global higher-order plate theory, Compos. Struct. 48 (2000) 231–244.
[76] K.N. Cho, C.W. Bert, A.G. Striz, Free vibration of laminated rectangular plates analyzed by higher-order individual-layer theory, J. Sound Vib. 145 (1991) 429–442.
[77] S. Shojaee, N. Valizadeh, E. Izadpanah, T. Bui, T.V. Vu, Free vibration and buckling analysis of laminated composite plates using the NURBS-based isogeometric finite element method, Compos. Struct. 94 (2012) 1677–1693.